DEVELOPMENT OF OPTICAL TAP FOR PLANAR LIGHTWAVE CIRCUITS AND INTRA-CHIP OPTICAL INTERCONNECT USING ION IMPLANTATION

By

Zhuo Chen

B.S. in Optical Engineering, Huazhong University of Science and Technology, 2000

M.S. in Optical Engineering, University of Central Florida, 2004

Submitted to the Graduate Faculty of

The School of Engineering in partial fulfillment

of the requirements for the degree of

Master of Science in Electrical Engineering

University of Pittsburgh

2006

UNIVERSITY OF PITTSBURGH

SCHOOL OF ENGINEERING

This thesis was presented

by

Zhuo Chen

It was defended on

November 20, 2006

and approved by

Dr. Joel Falk, Professor, Department of Electrical and Computer Engineering

Dr. Minhee Yun, Professor, Department of Electrical and Computer Engineering

Thesis Advisor: Dr. Kevin Chen, Professor, Department of Electrical and Computer Engineering

DEVELOPMENT OF OPTICAL TAP FOR PLANAR LIGHTWAVE CIRCUITS AND INTRA-CHIP OPTICAL INTERCONNECT USING ION IMPLANTATION

Zhuo Chen, M.S.

University of Pittsburgh, 2006

As silicon CMOS circuit technology is scaled above the GHz range, semiconductor industries face increasingly difficult challenges in implementing high speed metal interconnects. Metal trances are limited in density-speed performance due to the skin effect, electrical conductivity, and cross talk. However, optical based interconnects have much higher available bandwidth by virtue of the extremely high carrier frequencies of optical signals (>100 THz). As more and more optical lightwave circuits and intra-chip optical interconnects are fabricated, a compact, low loss optical tap technology is essential to incorporate optical interconnects into mainstream CMOS processes. A new tap device, which is based on optical refractive index variation induced by ion-implantation, has been found to especially promising.

In this thesis, an ion-implantation based device is introduced. BeamProp BPM simulations confirm a low excess optical loss over a wide range of tap length and ion implantation condition. An effort has been made to determine an optimal optical tap receiver design for integration with commercial CMOS processes. Low cost, ion-implantation based processing and single-mode waveguide make the new tap technology especially suitable for computer multi-chip module and for metro fiber to the home and desk telecommunications applications. Experimental results also show the feasibility of this tap device in today's demanding board level optical interconnect and semiconductor market.

TABLE OF CONTENTS

LIST OF TABLES

LIST OF FIGURES

ACKNOWLEDGMENTS

First and foremost, I would like to thank my advisor and friend Dr. Kevin Chen with my deepest gratitude. He is always there to help when I have difficulties in my research. Besides his comprehensive knowledge in Optoelectronics, his zeal for science, work ethic, patience and life attitude impressed me a lot.

I would also like to thank Dr. Joel Falk and Dr. Minhee Yun for serving on my thesis committee. Their willingness to share expertise and provide valuable advice is greatly appreciated.

I want to thank all my friends in Pittsburgh, for their support and friendship. A special thank should go to Dongxiao Li and Di Xu for their valuable help and discussions. I enjoyed working with all the members of Dr. Chen's group and expect to be a life long friend with them.

I want to thank my family, whose unconditional love and understanding supports me during the past two years. I would not be able to obtain this degree without their support.

1.0 INTRODUCTION

1.1 MOTIVATION

In a planar photonic device, optical signal are carried by an array of individual waveguides that have been fabricated on a planar substrate sealed within the package. For a number of applications in telecommunication and intra-chip optical interconnect, it is desirable to perform real-time optical monitoring in individual waveguides within the sealed package or directly on-chip. For application such as wavelength division multiplexing (WDM) a low-cost real-time optical monitoring technique becomes critical. In both metro and long-haul fiber-optical communication systems, optical signal is repeatedly amplified by in-fiber Er-doped fiber amplifier (EDFAs) to maintain proper signal-to-noise levels. While the number of channel in a WDM system increases, the total optical power carried by a single fiber or waveguide increase dramatically. Any optical power surge produced by optical amplifiers can be destructive to the entire system. Therefore, a low-cost and real-time optical power monitoring technique is needed to monitor optical power for individual fiber and waveguides in a sealed package. This is the first motivation of this thesis work.

As silicon CMOS circuit technology is scaled up in speed to the GHz range, the feature size of on-chip transistor is scaled down to sub-100 nm to accommodate more transistors and

computational power. The improvement of processing speed inevitably requires higher electrical power consumption and on-chip driving current density. On the other hand, the shrinkage of the feature size of on-chip metal interconnection poses severe limitation to the current density which can be carried by metal interconnect due to skin effect of metal wire and parasitic capacitors induced around the metal interconnect. These competing demands of higher processing speed and smaller feature size impose a serious challenge to the implementation of on-chip metal interconnects.

Electrical solutions include implementation of matched transmission line structures, repeater stages, higher conductivity copper trances, and lower capacitance, silicon-on-insulator (SOI) based circuitry. Each of these approaches can offer factors of about 1.5 to 2 performance improvement. Typical trade-offs on the other hand includes in terms of chip real estate, and increased processing costs.

In contrast to the electrical approach, optical based interconnects have been proposed that could fundamentally eliminate the bandwidth bottleneck of the metal interconnect. Optical interconnect has a number of orders higher bandwidth due to the extremely high carrier frequencies of optical signals. Optical signals can be carried over low-loss, low-latency, optical "trances" or waveguides, with little or no cross talk effects. To deliver optical signal to electronic circuits, an optical via is needed to tap an optical signal from optical waveguide backbone. The optical tap is a passive optical structure, whereby some portion of the light is collected at each tap point to feed on-chip electronic circuits, and the remainder is passed on to other taps in a series fashion. A typical optical tap application is optical clock distribution, whereby an optical clock signal is distributed via optical beams to multiple points on an electric circuit board or chip. This is the second motivation of this work.

Presently, the challenge is to implement the optical tap in a cost effective and compatible with standard IC fabrication techniques, so it can be readily integrated with CMOS devices. Tap designs based on integrated optics have the potential of serving this requirement, while also being directly compatible with planner light wave circuit (PLC) elements such as arrayed waveguide gratings (AWG) and frequency domain modulator (FDM). Planner tap designs are also compatible with silicon on insulator (SOI) based optical elements such as variable attenuators, modulators, and switches. In appreciation of CMOS chip real estate, any optical tap device design must also be as compact as possible.

In this thesis, we introduced a new tap design that incorporated a vertical ion-implantation structure for compact and efficient optical to electrical coupling between integrated optical waveguide layers and CMOS surfaces. Single mode transport allows future integration of wavelength multiplexing elements for maximum optical bandwidth utilization. The tap structure design was shown to readily integrate with traveling wave silicon photo detectors to extract the maximum possible speed from the CMOS technology.

1.2 THESIS ORGANIZATION

Chapter 2 contains an assortment of background information pertinent to this thesis. Included is a summary of schemes for different optical tap structures. Also found in this section is a treatise on ion-implantation with derivations for induced refractive index profile modification and other mathematics relevant to this discussion. A summary of various applications of ion-implantation can be found in this chapter as well.

Chapter 3 details the design and simulation of ion-implantation vertical optical waveguide taps utilized in the research herein. It begins with a detailed description of the SRIM calculation of ion implantation distribution and the TRIM calculation of damage distribution used for refractive index modification analysis. Details regarding the R-soft simulation with various implantation conditions are also presented along with relevant theoretical explanation of output characteristics of the device as well as the realization of the series cascade optical taps. Finally, the planer waveguide device applications, such as, FDM and AWG utilizing optical taps are discussed.

Chapter 4 contains experimental results obtained from the testing. Attention is given to the operational characteristics of the device. Careful comparison is made to transmission loss induced by the optical tap and the considerations are made regarding the significance of results obtained herein.

Chapter 5 contains a series of conclusions drawn from the data presented in chapter 3 and 4, as well as a summary of the work presented in this thesis. The chapter also contains a section on possible future work that would expand on the experimentation presented here and foster the completion of an inexpensive ion-implantation based optical tap suitable for a number of industrial and consumer applications.

2.0 BACKGROUND INFORMATION

2.1 APPLICATION OF OPTICAL TAP IN OPTICAL INTERCONNECT

The focus of this thesis is to develop a novel and CMOS compatible fabrication technique to fabricate on-chip optical taps. The optical tap is a passive optical structure, whereby some portion of the light is collected at each tap point to feed on-chip electronic circuits, and the remainder is passed on to other taps in a series fashion. Optical taps have two basic applications. First on-chip optical taps are essential devices for inter-chip and intra-chip optical interconnect for ultra-high speed electronic systems. A typical optical tap application in optical interconnect is optical clock distribution. Optical taps have also been used in the WDM communication system to monitoring the power variation in different signal channels. This chapter first provides some background information about the application of optical tap in optical interconnects and waveguide optical power monitoring. The current state-of-the-art on optical tap fabrications is reviewed. Based on the pro and con of the existing tap fabrication techniques, we propose to use ion implantation to fabricate on-chip optical taps for both intra-chip optical interconnect and WDM optical power monitoring.

2.1.1 Optical Interconnection For Electronics

Today, 0.18 μm CMOS technology enables a 3-GHz operational frequency for the Pentium 4 CPU. However poor wiring limits the data flow to only 533 MHz on the system bus. The overall performance of a computer is not limited by the speed of CPU, but by the ability to communicate rapidly between the CPU and other data processing units (memory and display chips). Although a copper connection can increase the connection speed, bit rates transmittable on electronic wires are fundamentally limited by the wire's parasitic resistance, capacitance, and inductance. Connection speeds will never keep up with a CPU running at 10 GHz. Further, transmission speed drops dramatically with the propagation distance.

Optical connections between circuit broads, electronic chips, and within one electronic chip are the ideal solution to remove this speed hurdle. Optical signals in free space or optical waveguides always travel at the speed of light independent of the size and the length of the optical wire (waveguide) and are free from electronic noise. For many high-end applications, an optical connection is the only connection technology that can keep up with the computation speed of the CPU. At present, optical connections between two computers are commercially available. It is predicted that optical communication within two computer broads (inter-board) will be available in 2-5 years; a chip-to-chip communication (inter-chip) will come onto the market within 5-10 years, while an on-chip optical connection within a VLSI electronic chip (intra-chip) might become available in two decades.

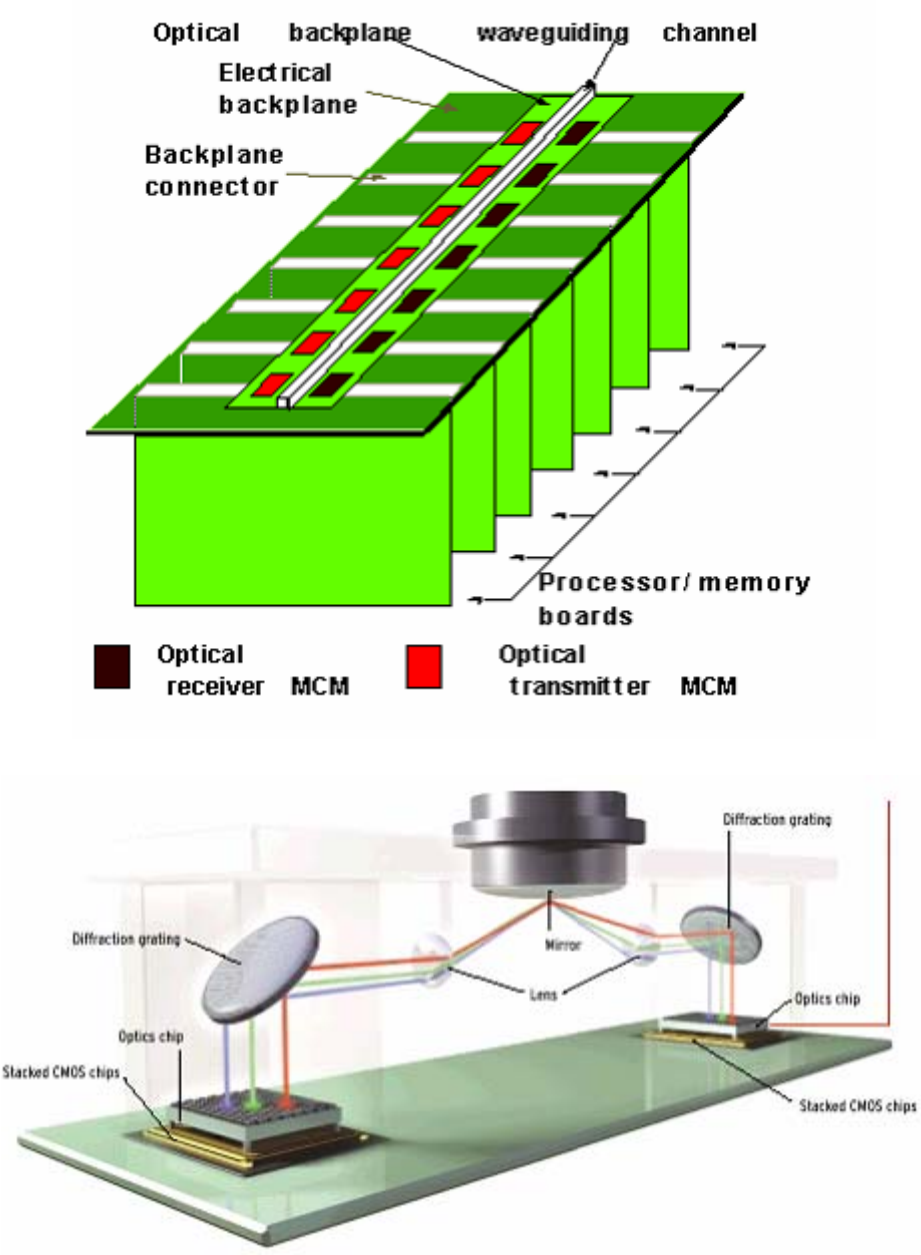

(a) (b)

Figure 1-(a) Demonstration of optical interconnection using optical backplane. (Inter-board) (b) Optical interconnection based on MEMS micro-optical devices (inter-chip). (© 1995 IEEE)

Figure 1a and b present two schemes proposed for inter-chip optical interconnect (1). A so-call optical back-plane technique proposed by R. Chen is shown in Fig. 1a, where high-speed

optical signal propagates in waveguide on a mother-board (optical backplane). On-board high-speed photo-diodes are used to detect evanescent guided optical wave and to convert optical signal to electric signal to support processor and memory boards mounted on the optical backplane. Free-space optical architectures using MEMS mirrors were also used for inter-chips optical interconnect as shown in Fig. 1b. However, both techniques only support inter-chips optical interconnect. It does not support a monolithic on-chip (intra-chip) optical interconnect. To deliver optical signal to various locations on-chip, optical vias (optical taps) are needed. An optical tap is a passive optical structure, whereby some portion of the light is collected at each tap point to feed on-chip electronic circuits, and the remainder is passed on to other taps in a series fashion. In the optical interconnection, an electrical signal will modulate a laser beam which propagates through a waveguide to a photodectector. The photodetector will in turn pass the optical signal to the electronics (2).

2.1.2 Optical Power Monitoring in Fiber Optical System

In a WDM optical communication system, optical signals propagates in one fiber are divided into many wavelength channels. Because the optical loss and gains gain of optical fiber amplifiers are wavelength dependent, variations in the optical power in different optical channel occur when multiple-channel optical signals transmit through one optical fiber. As a result of such variations, optical signal-to-noise (SN) ratio deterioration occurs in signals of lower optical power level. On the other hand, non-linear phenomena, such as four-wave mixing, occur in signals of higher optical power level, which deteriorates transmission signal waveforms.

In order to suppress such deterioration, it is vital that the system can control the uniformity of optical power level for each all optical channel (e.g. wavelength windows). The realization of an on-line network monitoring system which enables rapid failure localization, channel power equalization, and path restoration requires distributed network intelligence, i.e., utilization of optical node components with and embedded control function

The ideal optical signal monitoring devices should have low wavelength-dependent and polarization-dependent responses and should not introduce additional excess loss to the signal being monitored. To minimize the insertion loss, optical tap should be controllable to allow minimal necessary light be tapped out of optical channels. In one method, tap-waveguides are used to monitor optical signals traveling through the array of waveguides. As its name implies a tap-waveguide is a "spur" waveguide intersecting, or evanescently coupling with, a through-waveguide that taps off a small portion of the optical signal carried by the through-waveguide. The tapped portion of the signal is then carried to a photodiode or other sensing device. In many cases, the required tapping ratio is in the order of a few percent, resulting from a compromise between minimizing the insertion loss and achieving an acceptable signal-to-noise ratio at the detector.

However, given the constraints that all waveguides, including tap waveguides, lie in the same plane, that the waveguides may not be angled or curved too sharply, and the waveguides may not cross each other, the use of tap waveguides become increasingly problematic as planer photonic devices become more and more complex. To achieve optimum results, monitoring should be used throughout the entire transmission system, which requires the optical channel monitor devices to be compact, reliable, and low cost.

2.2 VARIOIUS OPTICAL TAPPING TECHNOLOGY

At present, several fabrication approaches have been experimentally demonstrated for the realization of optical tap have been proposed, that generally involve with a through-waveguide, a tap-waveguide and a photo-sensor. In this section, we briefly summarize the existing optical tapping technique for optical interconnect used in high-speed electronic system and fiber optical communication systems.

2.2.1 Optical Backplane Tap

Daimler-Chrysler Research is developing waveguide based optical backplanes to connect signals between circuit boards used in telecommunications (3). As in most optical interconnect schemes, the photons are generated by lasers as shown in Fig.2. The beam from a laser diode passes through one set of lenses, which expand the beam to a few millimeters in diameter. The expanded beam reflects off a micro-mirror before reaching a polymer waveguide entrance with great certainty, while at the waveguide exit, it is redirected by a mirror through another lens, which focuses it on a detector.

The DaimlerChrysler optical backplane relies on two features. The first is that guided wave propagates via the polymer waveguide within the backplane results in low link losses. The optical backplane is composed of an extended polymer waveguide structure and deflection micro-mirrors. The waveguides and micro-mirrors can be fabricated on arbitrary substrates such as material for printed circuit boards, glass PMMA and the micro-mirrors are integrated into the waveguides and lenses for focusing and collimation.

The second feature is that free space, expanded beam coupling between boards and backplane eliminates optical connectors. By expanding the beam diameter to a few millimeters, alignment tolerances in the range of $\pm$ 0.5mm can be achieved. Due to the relatively large waveguide cross section, imaging quality is not very critical and ball lenses will do. However, antireflection coatings should be applied for better imaging results. Plano-convex shaped lenses of high refractive index and aspheric plastic lenses can also be used to improve the image quality. The transmitter for the data transmission uses an edge emitting laser diode (780nm) with 1mW output power. And the receiver uses photodiodes with an active area that is slightly larger than a multimode glass fiber core.

This backplane optical interconnection is finally realized for a 55cm interconnection length. For each backplane, data transmission with a bit rate >1Gbit/s is demonstrated. The compact, connector-free and rugged concept is very well suited for applications in avionics and has the potential to be fabricated at low costs.

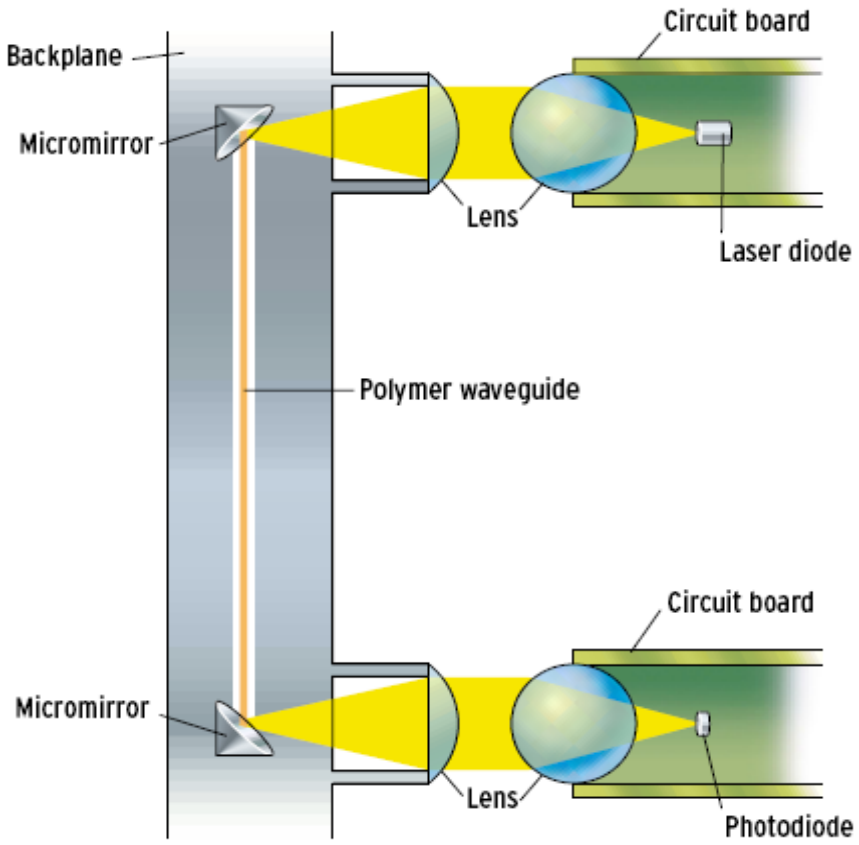

Figure 2-Backplane Optical Tap (© 1995 IEEE)

2.2.2 Vertical Receptacle Tap

Corning Inc. also proposed and patented an optical tapping technique; a tap–waveguide is optically coupled to the through-waveguide to tap a portion of the through-signal into the tap-waveguide. The tap waveguide is also a single-mode optical waveguide. A single-mode tap-waveguide is placed on either side of a single-mode through waveguide carrying optical signal. At the very beginning, the tap-waveguide locates very close and parallel to the through waveguide to couple a small portion (<1%) of the light to through-signal the tap-waveguide, as shown in Fig. 3. After a short coupling distance, the tap-waveguide moves away form the rail to

terminate the coupling effect. This system uses an optical waveguide "rail" to distribute optical energy to many taps and then the tap-signal can be detected by photodiode fabricated on the same lateral plane (4).

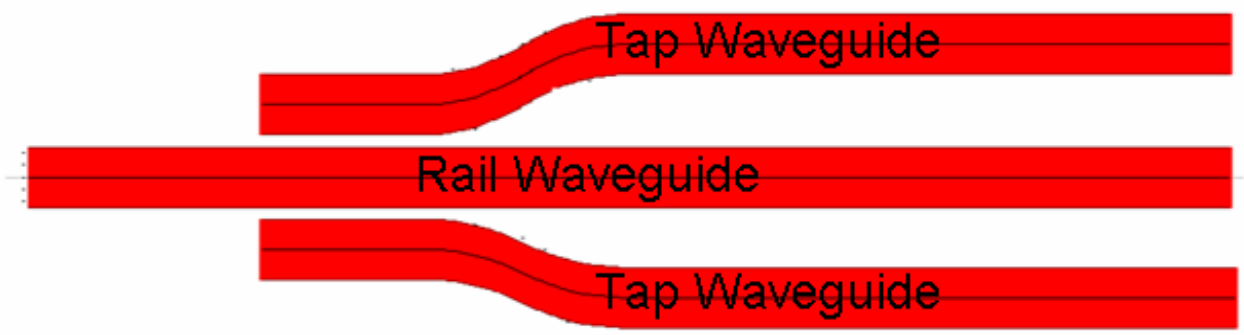

Figure 3-In Plane Coupling Tap

In order to detect the tap-signal entering the tap-waveguide, a tap receptacle is formed by isotropically etching a portion of the wafer. The tap receptacle has a "bowl" like profile and locates at the end of the tap-waveguide in order to collect the tap signal as shown in Fig. 4. The tap-signal is then reflected by the mirror on the interior wall of the tap receptacle and directed upward to the photodiode (5).

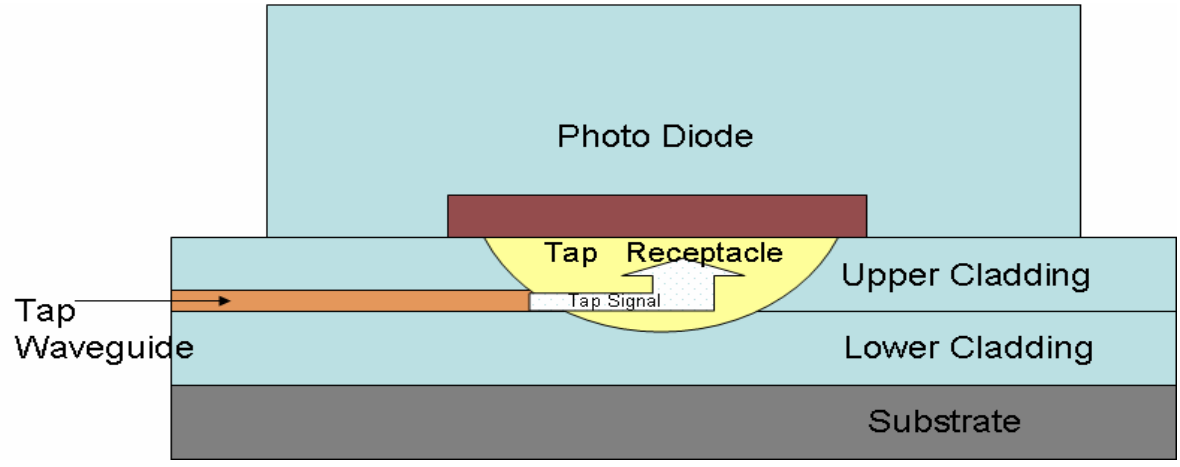

Figure 4-Vertical Receptacle Tap

To produce tap receptacle, other schemes were also used (6, 7, 8). It integrated 45-degree mirrors serving as a 90-degree out-of-plane optical deflector necessary to redirect the tap-signal vertically from a tap-waveguide to the photodiode. First, embedded optical waveguides were fabricated on silicon substrates with copper layers by spin-coating, photolithography and oxygen reactive ion etching. Next, 45-degree mirrors were formed by cutting the waveguide with a 90-degree V-shaped diamond blade. Finally, the polymeric optical waveguides were removed from the silicon substrates by wet etching the copper layers. The mirror losses were as low as 0.1dB for the single mode and 0.3dB for the multimode waveguide films, which showed that the mirror surfaces were very smooth. (Fig.5)

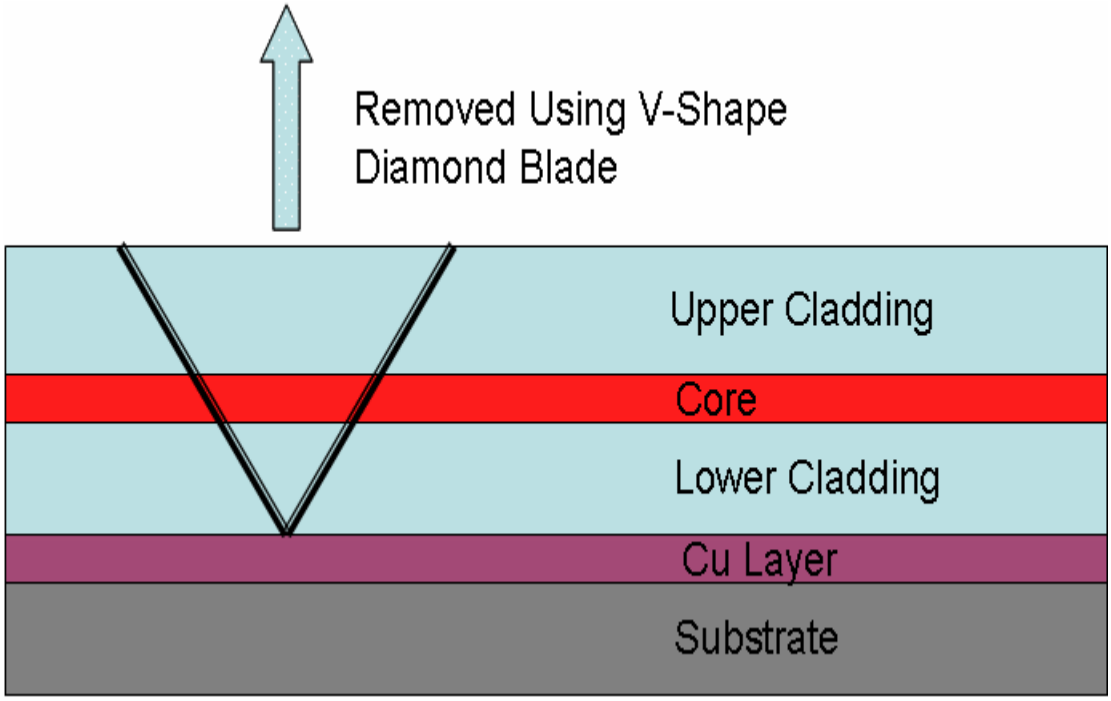

Figure 5-Integrated Mirror Tap

2.2.3 Grating Coupler Tap

Diffraction gratings used as on-chip optical taps to redirect guided light in a waveguide to on-chip photodiode integrated underlying to the waveguide as shown in Fig. 6.

Focusing grating couplers with a blazed grating profile are fabricated by electron-beam lithography by means of electron-dose control across the grating period. The signal beam at the specific diffracted wavelength is reflected, focused and directed to the photo detectors by the grating couplers. The grating and waveguide parameters can be optimized with respect to the coupling efficiency. For a coupling efficiency of more than 50% it is necessary to concentrate all the incoming light into the lowest diffraction order. This can be achieved by decreasing the grating period. The grating coupler with a coupling efficiency of much more that 50% is comparable with the coupling efficiency of prism couplers shown in Fig. 5.

The spot size of the focused light is another important issue to be addressed in the grating coupler design, which depends on the written grating pattern. Gratings without an aberration correction have a larger spot size than grating with a correction. This leads to a lower coupling efficiency.

Diffraction grating couplers are about to play an increasingly important role in miniaturized systems as they bring reduced size, and have the advantage of being compatible with wafer or board scale planar manufacturing processes. However, this allows a thicker isolation layer under the guide; even blazed diffraction gratings are relatively inefficient, with 30% or more excess loss typical. Also, grating couplers only allowing short distance optical data communication is another potential barrier to be overcome(9).

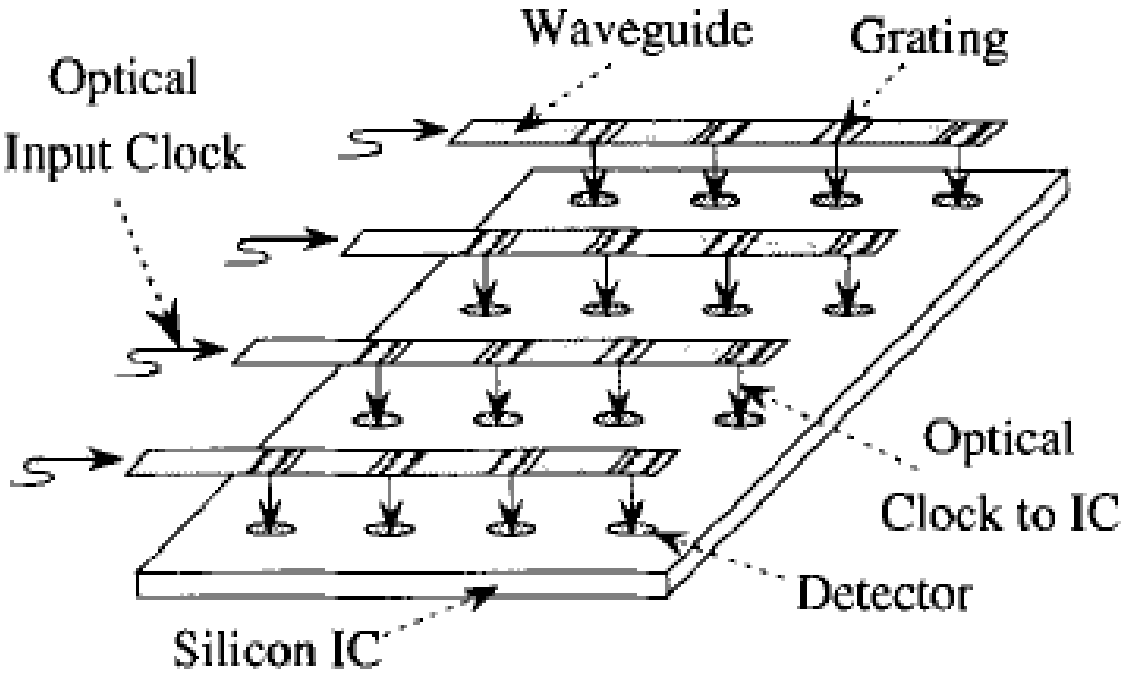

Figure 6-Grating Coupler Tap (© 1997 IEEE)

2.2.4 Waveguide Vertical Optical Tap

Most recently, a ridge waveguide based optical tap is realized incorporating multimode interference (MMI) scheme.(Fig.7) Polymers of refractive index of 1.5 and 1.4 were are used to fabricated the single mode waveguide core and cladding layers respectively due to their low optical loss, loss cost and easiness to be integrated to the CMOS fabrication process. The single mode guide has a 0.75 um core thickness and the tap region has a 1.5 um core thickness. The tap length was 15 um.

Before the tap, single mode through waveguide is used to be easily integrated to the WDM system. As light enters the tap region, multiple modes are excited due to the core

thickness increase. Furthermore, these excited multiple modes will interference with each other shifting the light profile towards the substrate. By adjusting the tap dimension, a controllable fraction of the through signal will be collected by the photodetector embedded in the substrate. The light profile then recovers back to the through waveguide to be used for the next tap. An antireflecting spacer layer is also fabricated to allow a good separation between the guides and the substrate.

2D and 3D simulation show <0.1 dB excess optical loss for the design, and a 40% optical coupling to the CMOS circuits. What is new in this technology is that it redirected some portion of the light vertically toward the substrate with little loss and short distance in a CMOS fabrication integration friendly manner. This technology is also compatible with grating assisted coupler to be used for inter board optical and intra chip level optical interconnect (10).

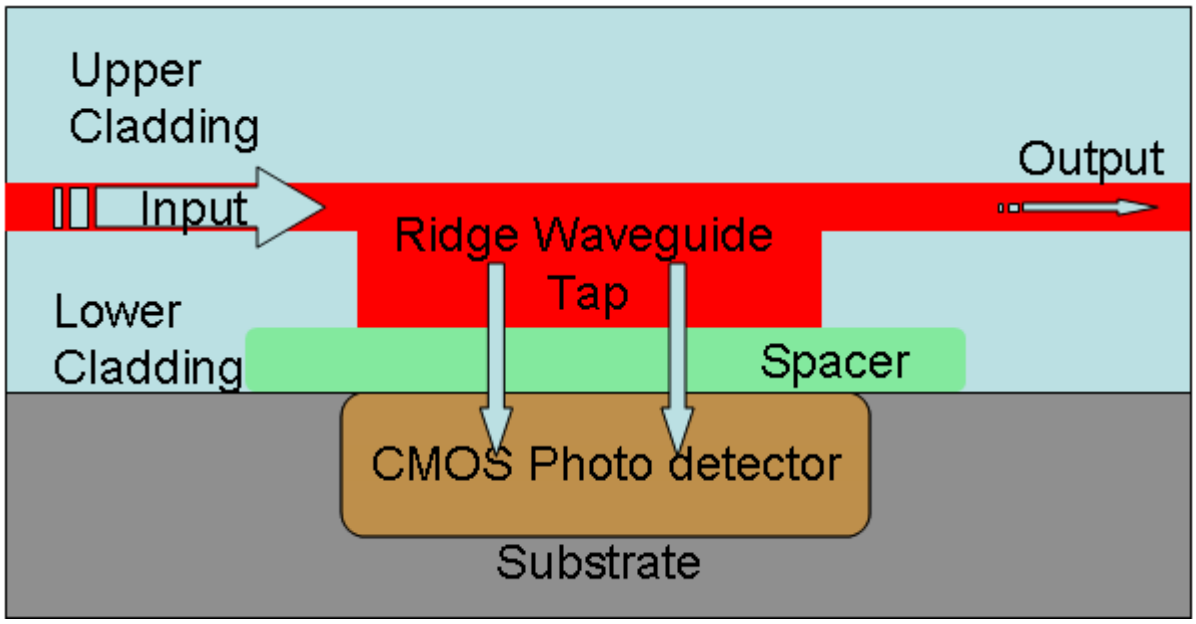

Figure 7-Ridge Waveguide Tap

2.3 A NOVEL OPTICAL TAP UTILIZING ION IMPLANTATION

To date, optical interconnects are typically multimode, and are routed over smooth surface. In-plane tap is the simplest to realized optical tap, but it will conflict with the real-estate constraint. Back-plane tap simply couples the light into the polymer waveguide, however, these three dimensional devices are not compatible with planar CMOS fabrication processes. Although, grating taps redirect laterally propagating light to a normal to surface direction for photo detection, diffraction gratings are relatively inefficient, with very large excess loss. Integrated mirror taps can introduce alignment issues.

Here, we introduced a new tap design (Fig.8) that incorporated a vertical ion implantation structure for compact and efficient optical monitoring and integration between optical waveguide layers and CMOS surfaces. The general procedure for forming an optical tap using ion implantation is to implant an optical material so as to increase the refractive index in a localized region. Before the tap, single mode transport minimizes the evanescent field profile so that there is little scatter and absorption loss. During the tap, light couple back and forth between the step index waveguide and the ion induced Gaussian profile index waveguide; at the same time, a portion of the light in the Gaussian guide starts to leak out because of the less than perfect confinement in the Gaussian guide. At the end of the tap, some portion of the light recovers back to the step index guide for single mode propagation; the rest of light continues to leak out because of lack of guidance (11).

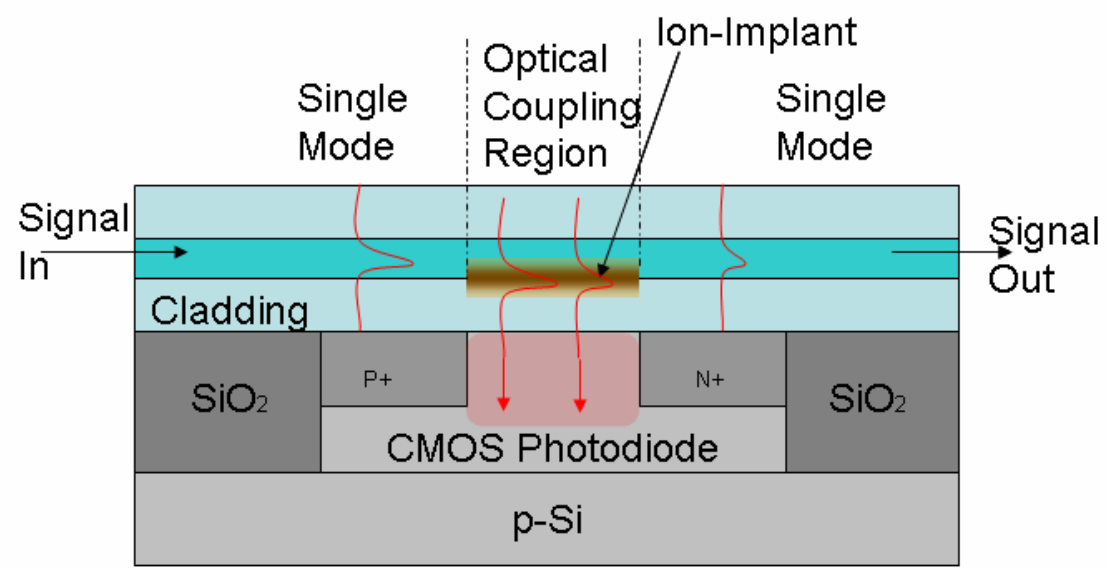

Figure 8-Ion Implantation Optical Tap

The advantage of ion implantation approach for optical tap fabrication is as follows:

1. Not Invasive, “Post” Processing;
2. Easy to Control, Adjustable Variables;
3. Vertical Tapping solved the real estate constraint;
4. Easy to integrate with CMOS devices.

2.4 APPLICATION OF ION IMPLANTATION

Ion implantation, as applied to semiconductor technology, is a process by which energetic impurity atoms can be introduced into a single-crystal substrate in order to change its electronic properties. Implantation is ordinarily carried out with ion energies in the 50 to 500keV range. Basic requirements for implantation systems are ion sources and means for their extraction, acceleration, and purification. This is followed by beam deflection and scanning prior to impingement on the substrate.

2.4.1 Introduction of Ion Implantation

Ion implantation provides an alternative to diffusion as a means for junction fabrication in semiconductor technology. The technique, however, has many unique characteristics which have led to its rapid development from a research tool to an extremely flexible, competitive technology (12).

There are two basic stopping mechanisms by which energetic ions, upon entering a semiconductor, can be brought to rest. The first of these is by energy transfer to the target nuclei. This causes deflection of the projectile ions, and also a dislodging of the target nuclei from their original sites. If E is the energy of the ion at any point x along its path, we can define a **nuclear stopping power** $S_n = (1/N)(dE/dx)_n$ to characterize this process. Nuclear stopping results in physical damage to the semiconductor, which takes the form of point as well as line defects. Often the semiconductor can become amorphous and/or semi-insulating as a result of this process.

A second stopping process is by the interaction of the ion with both bound and free electrons in the target. This gives rise to the transient generation of hole-electrons in the target. This gives rise to the transient generation of hole-electron pairs as energy is lost by the moving ion. We can define an **electronic stopping power** $Se = (1/N)(dE/dx)_e$ to characterize this process.

The average rate of energy loss with distance is then given by

$$-\frac{dE}{dx} = N[S_n(E) + S_e(E)]$$

Where N is the density of target atoms in the semiconductor. If the total distance traveled by the ion before coming to rest is R, then

$$R = \int_0^R dx = \frac{1}{N}\int_0^{E_0} \frac{dE}{S_n(E) + S_e(E)}$$

Where E_0 is the initial ion energy. The quantity R is known as the range. A more significant parameter, of interest in semiconductor technology, is the projection of this range along the direction of the incident ion, as shown in Fig.9. Because of the statistical nature of this process, **this projected range** is characterized by its mean value Rp, as well as by a standard deviation ΔRp along the direction of the incident ion. This latter term is refereed to as the straggle (13).

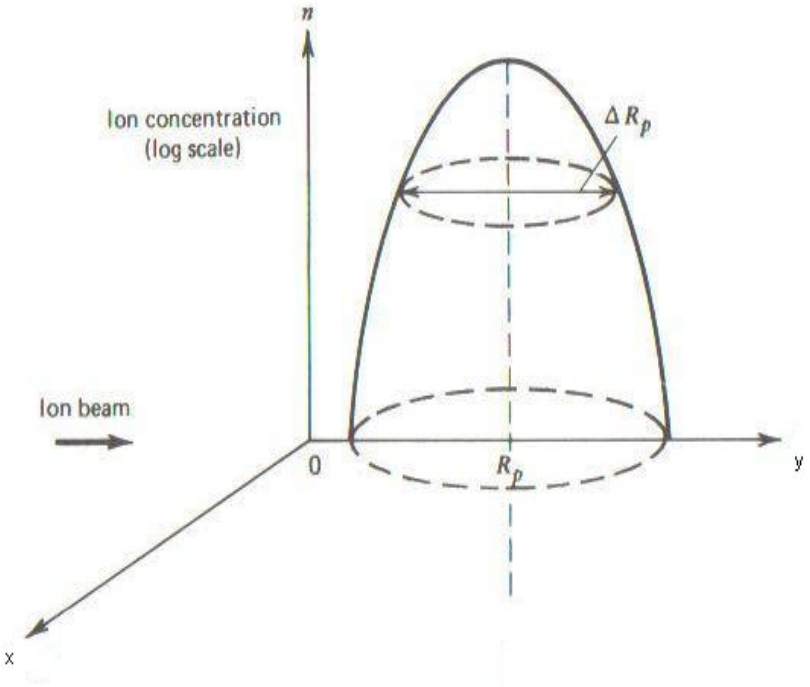

Figure 9-Range and Straggles

In practice, the ion beam also has a spread at right angles to its incidence. This **transverse straggle** is denoted by ΔRt , and is of importance in determining the doping distribution near the edge of a window which is cut in a mask. Transverse straggle can be ignored if the width of this window is large compared to the implant depth (14). For this case, the statistical distribution for an amorphous target can be described by a one dimensional Gaussian distribution function of the form

$$\phi(x) = \exp[-\frac{1}{2}(\frac{x-\bar{x}}{\sigma})^2]$$

Where $\bar{x}$ is the mean value and σ is the standard deviation. Integration of this function over the limits $\pm\infty$ results in the dose. Writing this dose as Q_0 ions cm^{-2} and noting that

$$\int_0^{\infty} e^{-z^2} dz = \frac{\sqrt{\pi}}{2}$$

The impurity distribution is given by

$$N(x) = \frac{Q_0}{(2\pi)^{1/2} \Delta Rp} \exp[-\frac{1}{2} (\frac{x - Rp}{\Delta Rp})^2]$$

This function has a maximum at Rp, and falls off rapidly on either side of this mean value.

2.4.2 Ion Implantation Induced Refractive Index Change

Ion beam implantation and irradiation have been used extensively to change the optical properties of dielectric and semi-conducting materials. In particular, material changes induced by exposure to ion beams can be used to change the refractive index and, hence, to define optical waveguides. Using this technique waveguides and waveguide lasers have been fabricated in a wide range of materials (15).

Radiation-induced changes of refractive index can be attributed to several mechanisms. Of these mechanisms, two of which have been considered are ionizing radiation, and displacement creation by atomic collisions. Other possible effects, such as those connected with ion implantation and chemical combination of the incident particles with the target material, are not considered here.

Ionizing radiation such as gamma rays and electrons induce absorption band (color centers) which have an associated index change. It has been found experimentally that this index change is small, typically of the order of 10^{-4}. Irradiation with various types of particles such as

neutrons, protons, and other ions changes the density and hence the refractive index of a material. The index change in this case can be considerably greater, changes from 0.001 to 0.2 having been reported. It has generally been assumed that these changes are caused predominately by atomic displacements and that the effect of ionization on the index is negligible.

In order to relate the index change to dosage for proton irradiation of fused silica, empirical data from proton irradiation have been utilized. These data relate the index change to proton dosage, from which the change with displacement density can be computed. From TRIM, the index change with dosage can be determined for any type of radiation. For fused silica, the saturation dosage results in a positive index change of about 0.01.

The refractive index profile for proton irradiation of fused silica can now be determined by calculating the density of displacements (damages) as a function of position in the material. When a proton passes through fused silica it gives up energy both by ionization of the atoms and by atomic displacements. In order to determine the distribution of displacements, it is convenient to consider two regions, an ionization region in which the proton loses energy primarily by ionization, and a collision region in which the proton loses energy primarily by the creation of displacements. The transition between these two regions is gradual, but the result is not significantly affected if an abrupt transition is assumed.

In the ionization region most of the proton energy is given up by ionizing the atoms in the fused silica, which does not cause a significant change of the refractive index. However, some displacements are produced, the cross section for displacements being inversely proportional to the proton energy. The density displacements in the ionization region is given by

$N = kD/E$ (displacements per cm^3),

Where D is the dosage in protons per cm^2 and E is the proton energy in MeV. The constant of proportionality k has been estimated from data obtained with proton irradiation of silicon, and has a value of about 8000.

At the end of the range, the remaining energy is given up primarily through collisions with the atoms of the fused silica, which create atomic displacements; this region is called the collision region. The length of the collision region for a single proton is less than 0.1 um. There fore, the only significant density of displacements, in both the ionization and collision regions, occurs in a region less than one-half micron long. Thus the profile of displacement density for a single proton is simply a narrow channel less than one-half micron long located at the end of the range.

To determine the density of displacements N for a many-particle beam, the effects of range straggling must be considered. Since the ionization process which determines the proton range is random, not all particles of the same incident energy have exactly the same range. Rather, there is a Gaussian distribution of ranges, about the mean, where σ (the standard deviation of the Gaussian distribution) is a known function of the energy. In general, the standard deviation of the range straggling for a many-particle beam, is greater than the length of the displacement channel for a single proton, and the distribution of displacements within that region is determined by the range straggling.

The consideration of range straggling indicates that a mono-energetic beam of many particles will create a displacement channel having a refractive index profile of Gaussian cross section with standard deviation σ. The density of displacements at the peak of the Gaussian channel will depend on the total number of displacements and the width of the Gaussian channel

(proportional to σ). As an approximation, we assumed that all of the displacements are created in the collision region.

The distance of the end of range below the irradiated surface increases with ion energy and decreases with atomic number of the ion. The mechanism by which the refractive index is modified is highly dependent on the type of material being irradiated. In essentially amorphous dielectric materials such as fused silica, for example, irradiation with ions leads to breaking of intermolecular bonds in the nuclear damage region. This produces further amorphorzation of the material and an increase in density, and hence, refractive index, at the end of range of the ions. This then creates a waveguide region buried below the irradiated surface, the depth depending on the ionic species and its energy.

2.4.3 Application of Ion Implantation In Optical Waveguide

Due to controllability of the implantation process, in terms of doses, energies, ion types and temperature, numerous commercially interesting possibilities such as the formation of waveguides and waveguide devices buried well below the surface of the substrate (16).

By using ion-implantation, direct-writing optical waveguides have been fabricated in a wide range of materials as in Fig.10.

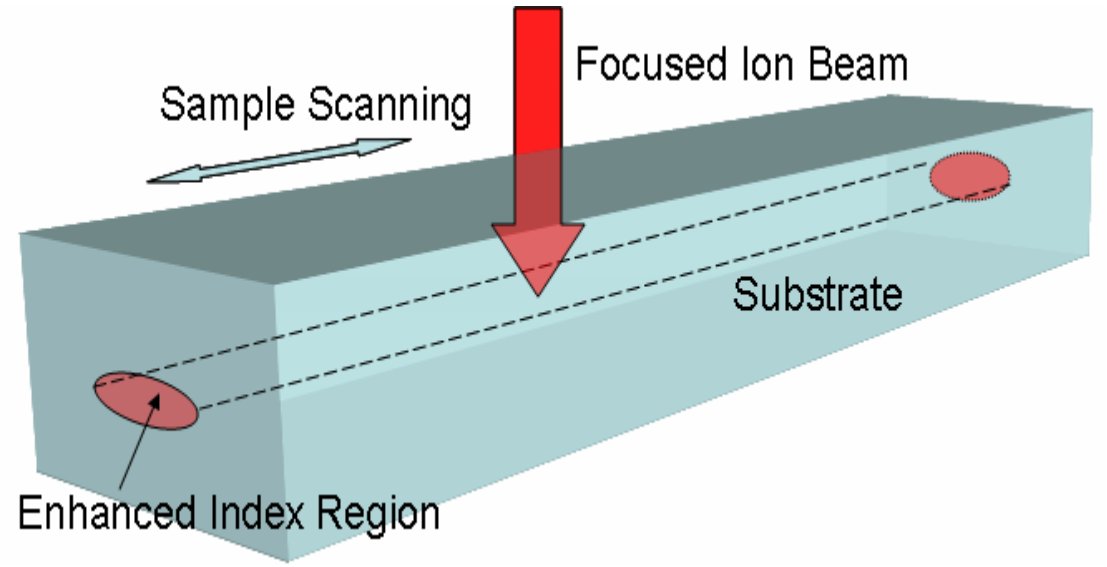

Figure 10-Ion Implantation Waveguide Fabrication

The ions (H+) were focused through magnetic quadrupole lenses. The depth of the waveguide below substrate surface can be controlled by the ion injection energy. The width of the waveguide depends on the longitudinal "straggle" of the ions. This "direct-writing" technique not only eliminates the need for a thick mask, but also has the possibility to locally selectively modify refractive index to improve the device performance. The technique is most suitable to fabricate waveguides and devices in materials where the irradiation increases the refractive index.

This technique can also be utilized to fabricate long-period gratings in optical fibers as shown in Fig.11. Most popular grating fabrication methods require photosensitization of the fiber before the grating is produced by irradiation of the fiber with strong UV laser irradiation by use of either an optical phase mask or interferometric method. Other techniques that have been demonstrated for the production of long period gratings include the introduction of periodic microbends into the fiber by use of electric arcs and physical deformation of the fiber. However, Ion implantation technique allows many different grating profiles to be fabricated, since it is a

direct-write technique and the index of individual grating elements can be controlled in a straightforward manner. This type of control is not possible with any scheme relying on a mask before exposure. Most recently, masked ion implantation with 5.1MeV He2+ ions was demonstrated as an alternative fabrication method for long-period gratings. The fiber was etched so that the 5.1MeV He2+ ions were implanted within the core (17).

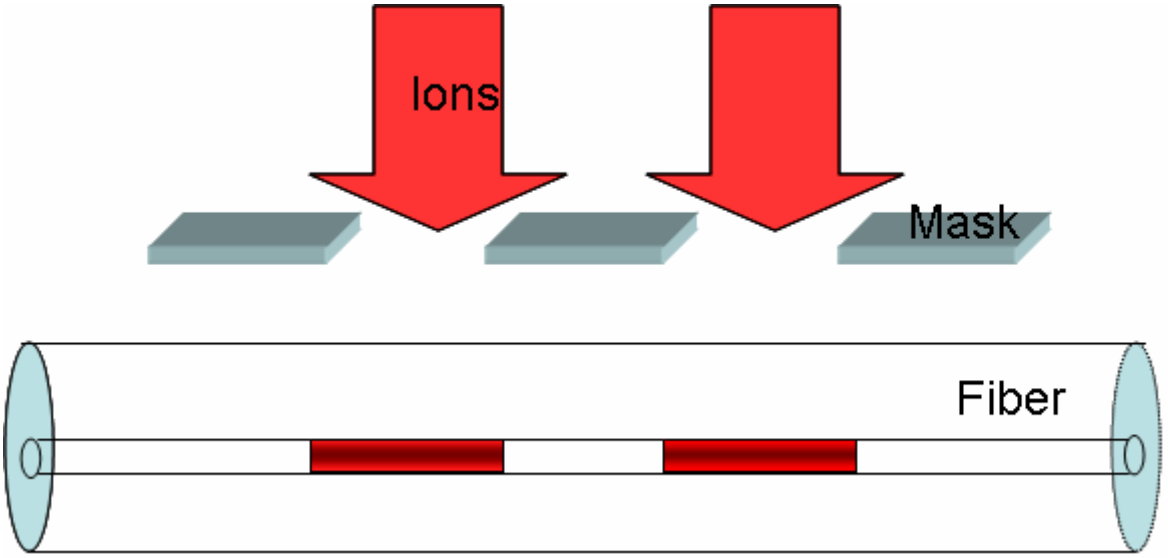

Figure 11-Long Period Grating Fabrication using Ion Implantation

The stopping distance of He2+ with this energy in silica is only about 24um; however, the distance from the center of the core to the surface of an unetched optical fiber is significantly greater. H+ ions with energy of 2.4MeV, however, have a stopping distance in silica of approximately 62.5um, and so significant index changes can be produced in the core of a standard 125 um fiber with no preparation of the fiber other than removing the plastic coating.

Another approach of using proton to fabricate LPG without removing the plastic coating is demonstrated recently. A 25mm length of fiber was stripped of its jacket. The fiber were then mounted within the microprobe target chamber and irradiated with a focused beam of protons

produced by a 5U pelletron accelerator. To fabricate a grating element, we held the fiber stationary while it was exposed to the fixed focused beam. After each exposure, the fiber was translated along its axis by a distance equal to the grating period.

There are several advantages to using ion implantation rather than existing techniques to produce gratings. First, the index of any commercially available silica fiber can be changed by use of ion implantation and thus the use of specially prepared photosensitive fiber is not required. Second, at the ion doses that are required for fabrication of gratings, the index change is approximately linear with ion dose. This linear index change eliminates the necessity for complex irradiation schemes of the type required for UV irradiation of photosensitive glasses, which have a nonlinear response, to produce gratings with well-characterized refractive index profiles. Finally, the refractive index change produced in silica by ion irradiation is known to be stable to above 500 degree C, and this fact may present significant advantages in certain sensing applications.

Ion implantation can also be used to create unbalanced Mach-Zehnder Interferometer (MZI) based coarse WDM device using fused biconical tapered (FBT) couplers as shown in Fig.12.

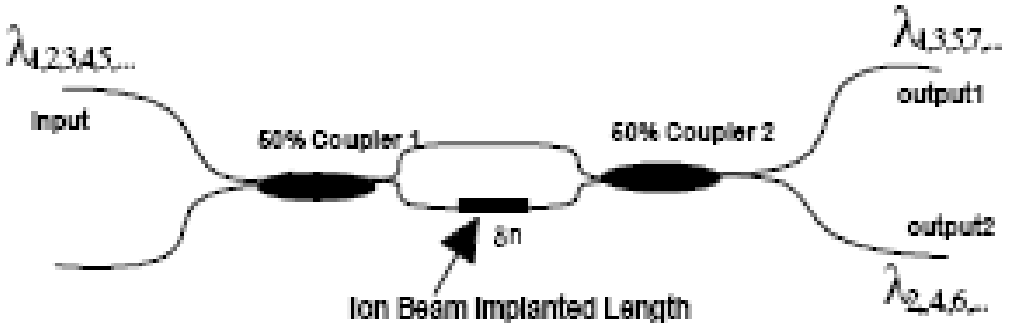

Figure 12-Mach-Zehnder Interferometer Fabrication using Ion Implantation

Unlike DWDM components the channel spacing in CWDM devices is very large and hence imposes much tighter tolerances in precisely inducing a small phases difference in the optical path of a MZI. This could be achieved by either creating an optical path difference or an index change between the two arms of the device. In this demonstration, H+ ions of 2.476 MeV energy with beam doses of $1-5\times10^{16}$ ions/cm2 are implanted into an arm of a MZI for inducing a precise refractive index change between the two arms to create CWDM components of highly controlled wavelength channel spacing (18).

Another important aspect of applying an ion beam implanted fiber to create an unbalanced MZI with coarse channel spacing is its lower sensitivity to temperature and environmental changes. For dense channel spacing, temperature fluctuation induces more unbalance between the two arms of a MZI formed using the path difference method. This results in wavelength channel shifts and thus the need for active or passive thermal compensation schemes.

3.0 ION IMPLANTATION TAP DESIGN AND SIMULATION

In this thesis, ion-implantation was used to realize an on-chip optical tap. Ion implantation has been used extensively to produce waveguide. For those applications, the propagation loss was minimized for guided wave applications. On the contrary, the fabrication of optical tap aims to increase local optical loss in particular section of waveguide to tap small portion of light out for power monitoring or signal extraction. Two mechanisms could contribute to the increase of optical loss due to the ion implantation. First, the injection of various ion species increases the refractive index in the vicinity of embedded waveguide, which disturbs the guided mode and produce optical loss. The second mechanism contributes to the optical loss might arise from increase scattering loss due to the injection of ion. High energy ion implantation might cause damage and produce scattering center between optical waveguide cladding and the core. However, various reports on fabrication of ion implanted waveguide has shown that the propagation loss of implanted waveguide can be as little as 0.1 dB/cm, the scattering loss in a section of 10-100 μm tap could be ignorable. Therefore, the simulation work described in this chapter focus on the first mechanism.

3.1 PROPOSAL OF ION IMPLANTATION BASED OPTICAL TAP

3.1.1 Novel Tap Design

The waveguide structure chosen for simulation was silica-on-silicon waveguides. The upper and lower cladding material is made of fused silica SiO2 with refractive index of 1.46. The thickness of the cladding layer is 48um. The core is made of 3% Ge doped SiO2 with slightly higher index 1.465 with Δn=0.005. The width of core is 8um. Based on this waveguide dimension, only a single mode can be supported by the waveguide at the telecommunication wavelength at 1550 nm.

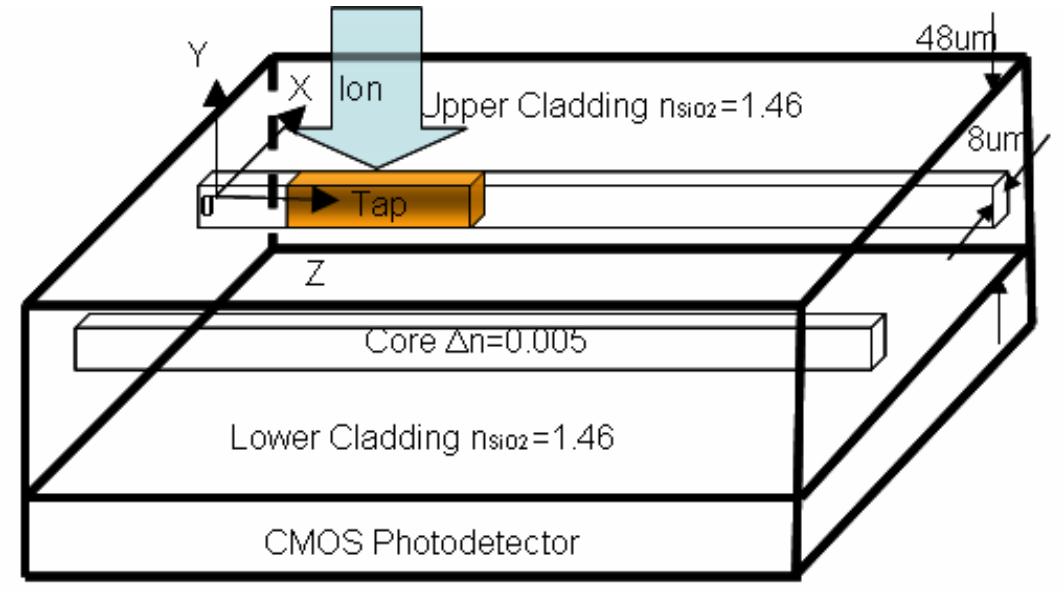

Figure 13-Vertical Ion Implantation Tap Structure

It would also be within the spirit of the present design to form a tap structure directly below the through-waveguide, without fully interrupting the through waveguide. At the tap structure, Ions were vertically implanted in the core as well as the cladding causing the

redistribution of the waveguide refractive index profile. Fig.13 shows a cross sectional side view of a tap monitoring system according to the present design with the coordinate origin locates at the center of the core.

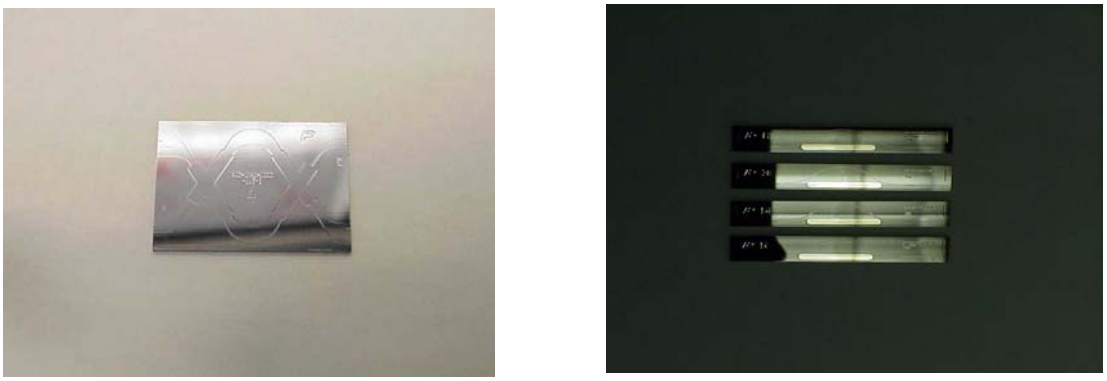

(a) (b)

Figure 14-(a) Array Waveguide Grating (b) Mach-Zenhder Interferometers

Base on the simulation results we obtained in this chapter, two different silica-on-silicon waveguide structures was chosen for the experiment. They are a Mach-Zenhder interferometers and an array waveguide grating. Figure 14 show photographs of both waveguide structures. The experiment demonstration of optical tap will be described in Chapter 4.

In this embodiment, a small portion of the light will be extracted from the through signal at the optical tap and collected vertically at very low excess loss for optical channel monitoring as shown in Fig.15. The amount of light coupled into the tap would depend on the depth and length of the tap structure.

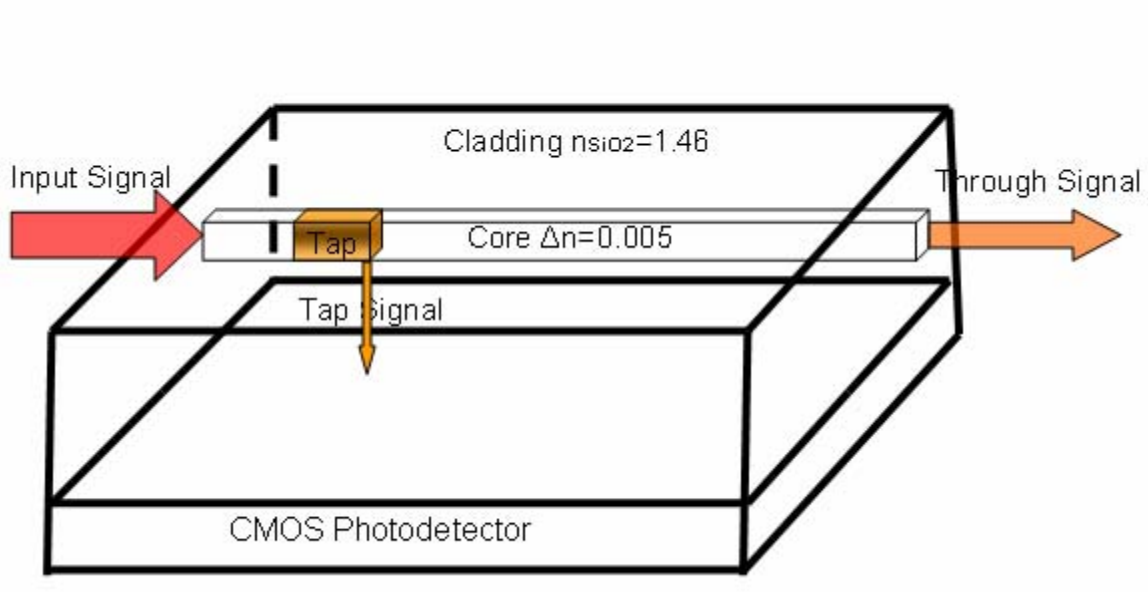

Figure 15-Mechanism of Tap Operation

To form an optical tap, it is necessary to determine the amount of index changed introduced by the implantation and the size and shape of the affected region. In the case of uniform irradiation of a flat surface of a material, the index profile in the direction parallel to the incident radiation must be determined.

It is indicated that the refractive index change is proportional to the ion distribution of the implantation. And it can be described by the following equation (13).

$$\Delta n = (\Delta n_{peak}) \exp[-\frac{1}{2}(\frac{y - Rp}{\Delta Rp})^2]$$

Where Rp is the projected range controlled by the ion energy, ΔRp is the straggle decided by the ion species, Δn_{peak} is the peak index change controlled by the ion dosage. After the ion implantation is refractive index profile at the optical tap becomes the overlap of the original step index profile and the ion-induced Gaussian index profile as shown in Fig.16 and 17

Here we have 4 variables to control the optical tap Rp , ΔRp , Δn_{peak} and tap length.

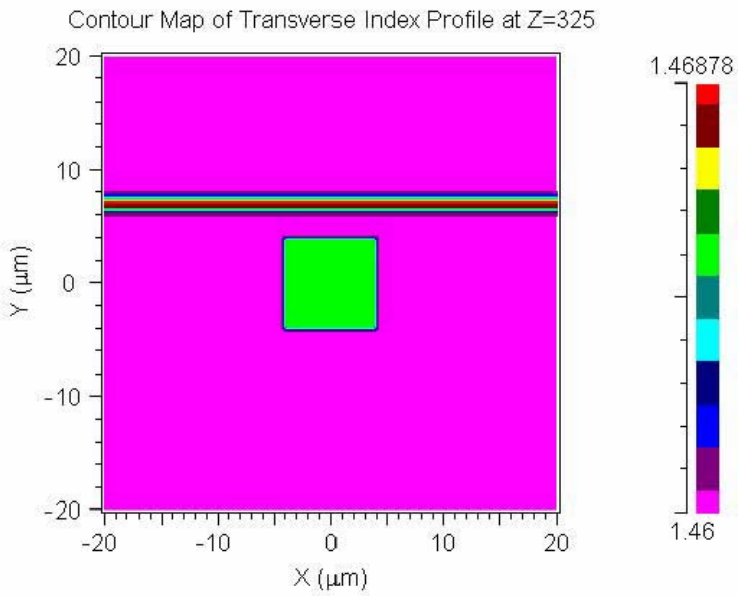

Figure 16-Cross-section View of Step Index Waveguide and Ion Induced Refractive Index Profile Change

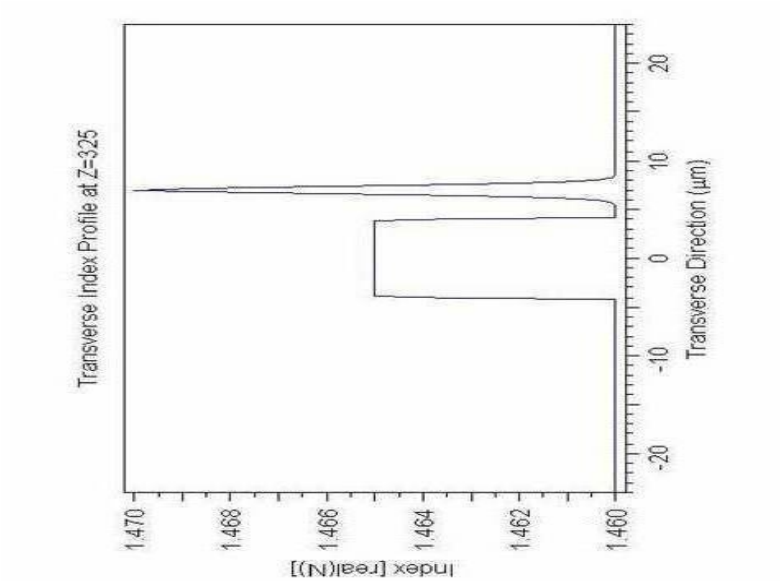

Figure 17-Illustration of Ion Induced Refractive Index Profile Change On Step Index Waveguide Core

3.1.2 Tap Fabrication

Fig.18 shows a flowchart of a method for constructing a planar photonic device embodying the present design, the method comprising the following steps:

a) Fabricating a CMOS light sensor embedded in the silicon substrate for sensing light that has entered the tap.

b) Laying down an under-clad layer and waveguide core layer;

c) Etching waveguides into the waveguide material;

d) Laying down an over-clad layer on top of the waveguides;

e) Ion implanting a tap-waveguide to optically couple a portion of an optical signal carried by the through waveguide and diverts it into the tap-waveguide.

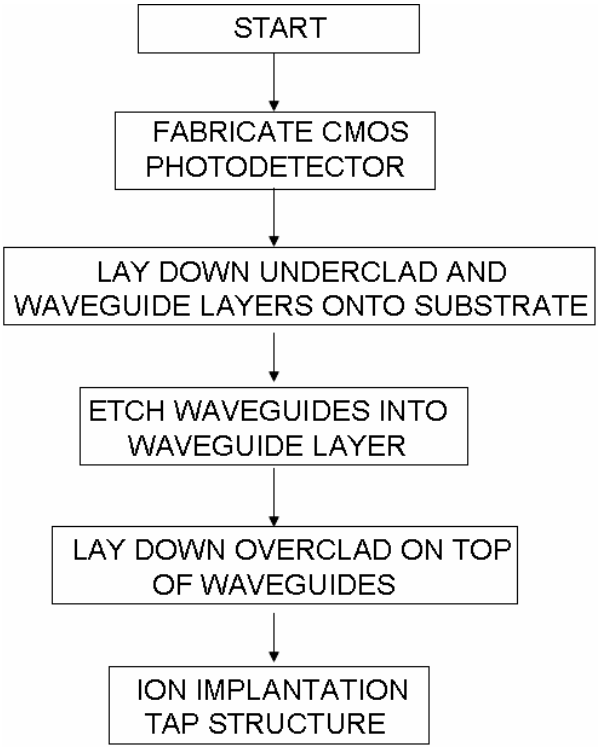

Figure 18-Flowchart of Optical Tap Fabrication

3.2 ION IMPLANTATION CONDITION CALCULATIONS

To produce optical tap, the profiles of implanted waveguides were first determined. In this thesis, SRIM program developed by IBM was used to simulate implanted ion and damage distributions. SRIM is a group of programs which calculate the stopping and range of ions (10 eV - 2 GeV/amu) into matter using a full quantum mechanical treatment of ion-atom collisions. This calculation is made very efficient by the use of statistical algorithms which allow the ion to make jumps between calculated collisions and then averaging the collision results over the intervening gap (19). During the collisions, the ion and atom have a screened Coulomb collision, including exchange and correlation interactions between the overlapping electron shells. The ion has long range interactions creating electron excitations and plasmons within the target. These are described by including a description of the target's collective electronic structure and inter-atomic bond structure when the calculation is setup. The charge state of the ion within the target is described using the concept of effective charge, which includes a velocity dependent charge state and long range screening due to the collective electron sea of the target.

3.2.1 SRIM Ion Distribution Prediction

Table 1 shows the SRIM theoretical prediction of projection range and straggle of ion distribution corresponding to some certain implantation energies when proton and boron ion bombard fused silica materials.

Table 1- Comparison of SRIM calculation under different ion energy

H+ bombard SiO2

Ion Energy	Range Rp	Straggle ΔRp
550.00 keV	6.24 um	2971 A
700.00 keV	8.81 um	3928 A
1.00 MeV	14.97 um	6897 A
1.50 MeV	27.70 um	1.16 um

B11+ bombard SiO2

Ion Energy	Range Rp	StraggleΔRp
550.00 keV	1.30 um	1538 A
700.00 keV	1.51 um	1603 A
1.00 MeV	1.87 um	1698 A
1.50 MeV	2.4 um	1797 A

The choice of proton over other bombard particle in our tap fabrication is based on the following reasons:

a) Relatively easy to achieve high dosage.

b) Large amount of data available to determine the induced refractive index change Δn_{peak}

c) Projection depth Rp is deep at relatively low injection energy because of the low mess

d) Straggle ΔRp is relatively small and only local index modification will be introduced

3.2.2 TRIM Damage Calculation

TRIM calculation is also conducted to decide the atom displacement (damage) distribution which is the main reason for the refractive index modification induced by the ion implantation. Table 2 shows the TRIM re-calculation of proton projection range and silica damage range based on 3000 ions implantation under different ion energies.

Table 2-TRIM calculation of projection range and silica damage range

H+ energy(MeV)	SRIM approximation H+ range(um)	TRIM Simulation (3000 ions samples) H+ range recalculation(um)	SiO2 Damage range(um)
1.0	14.97	15.3	15.3
1.1	17.28	17.7	17.7
1.2	19.7	20.1	20.1
1.3	22.24	22.8	22.5
1.4	24.91	25.5	25.2
1.5	27.7	28.2	27.9
1.6	30.61	31.15	31.15

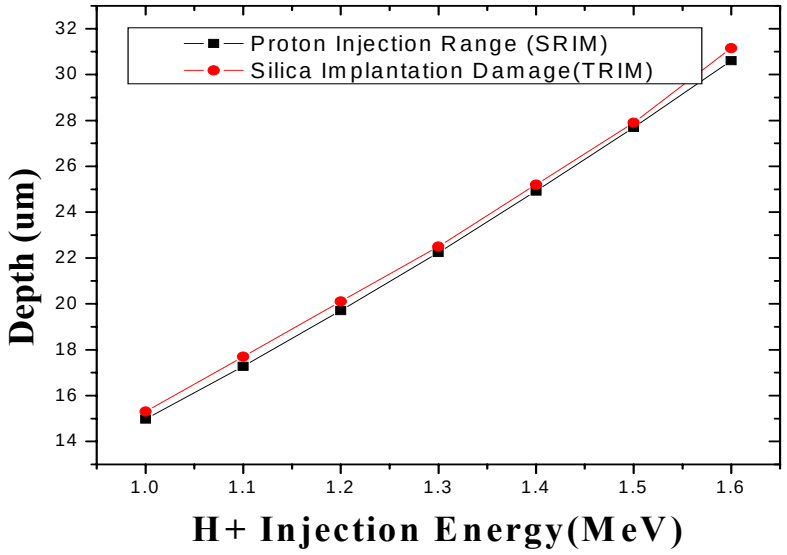

Figure 19-Comparison of SRIM and TRIM Results

Table 2 shows very little difference between the SRIM theoretical prediction and TRIM calculation. This is also shown in the following comparison plot Fig. 19.

3.3 TAP DESIGN AND SIMULATION

Several simulations were run for various aspects of the proposed waveguide tap optical design. The goal was to establish the theoretical feasibility of the proposed tap technology on CMOS circuits. All numerical simulations were conduced using Rsoft's BeamProp software version 6.0.4.2 (RSoft,Inc., Ossining, NY 10562 USA) with full transparent boundary conditions.

3.3.1 Basic Tap Operation

The basic theory of operation of the ion-implantation based optical tap is as follows (as shown in Fig.20):

1. Before the tap, single mode propagation of guided wave minimizes the evanescent field profile so that there is little scatter and absorption loss.
2. When guided waveguide propagate into the optical tap, depending on refractive index change caused by ion implantation and the location of implanted waveguide. The tap region becomes a multi-mode waveguide and guided light couple back and forth between the fundamental mode and higher order modes. At the same time, the peak location of the fundamental mode also shifts toward ion implanted region. Both mechanisms contribute to the mode mismatch between ion-implanted region (optical tap) and embedded step-index waveguide.

3. At the end of the optical tap, light guided in implanted waveguides will leak out due to lack of guiding and subsequently is received by integrated photo detectors. The mode mismatching between ion implanted regions and embedded step-index waveguide will also contribute to optical loss.

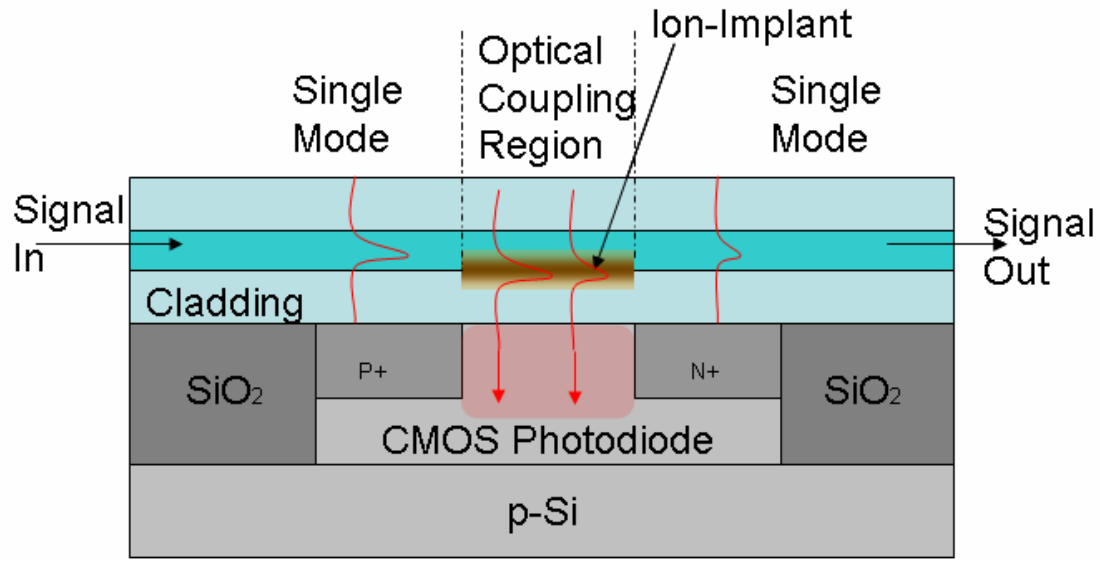

Figure 20-Side Cross-sectional View of the Proposed Optical Waveguide Tap

The following simulations for tap operation with different variables will reveal the important trends for various aspects of the proposed waveguide tap optical design.

If the refractive index change induced by ion implantation is strong enough, the implanted waveguide will support a guided mode at 1550 nm. If the implanted waveguide is produced close to the step index waveguide or in physical contact with the step-index waveguide, part of guided mode will be coupled into the implanted region.

According to directional couplers theory, a light wave launched into one of the waveguide couples completely into the opposite guide. But once the light has crossed over, the wave couples back into the first guide so that power is exchanged continuously as often as the

length of the device permits. However, complete exchange of light power is only possible between modes that have equal phase velocities or, equivalently, equal propagation constants, e.g. the two guides should be identical.

In this situation, the tap is actually composed of a step index through waveguide and Gaussian index tap waveguide placed near each other as shown in Fig.21. When the peak refractive index change of implanted waveguide is large enough to support guided mode at 1550 nm, the tap compound structure is no longer a single mode structure. Instead, the implanted regions should be viewed as an integrated composite guided structures. Similar to a coupler, it supports an even and an odd mode. Since the implanted waveguide has different propagation constant from the step-index waveguide, only partial energy exchange take places between the even and the odd modes. At the beginning of the optical tap or the input end of the composite waveguide, two waveguides were excited with their own modes, the superposition of both fields constitute odd and even modes. Since propagation constants for implanted waveguide and the step index waveguides are different, when both of them travel along the tap region, the relative phase difference continuously evolves from constructive interference (even modes) to destructive interference (odd mode). It thus appears that the light power switches from implanted waveguide to the step-index guide. In the following section, we use the peak index of Δn_{peak} =0.005 to illustrate the idea (20, 21, 22).

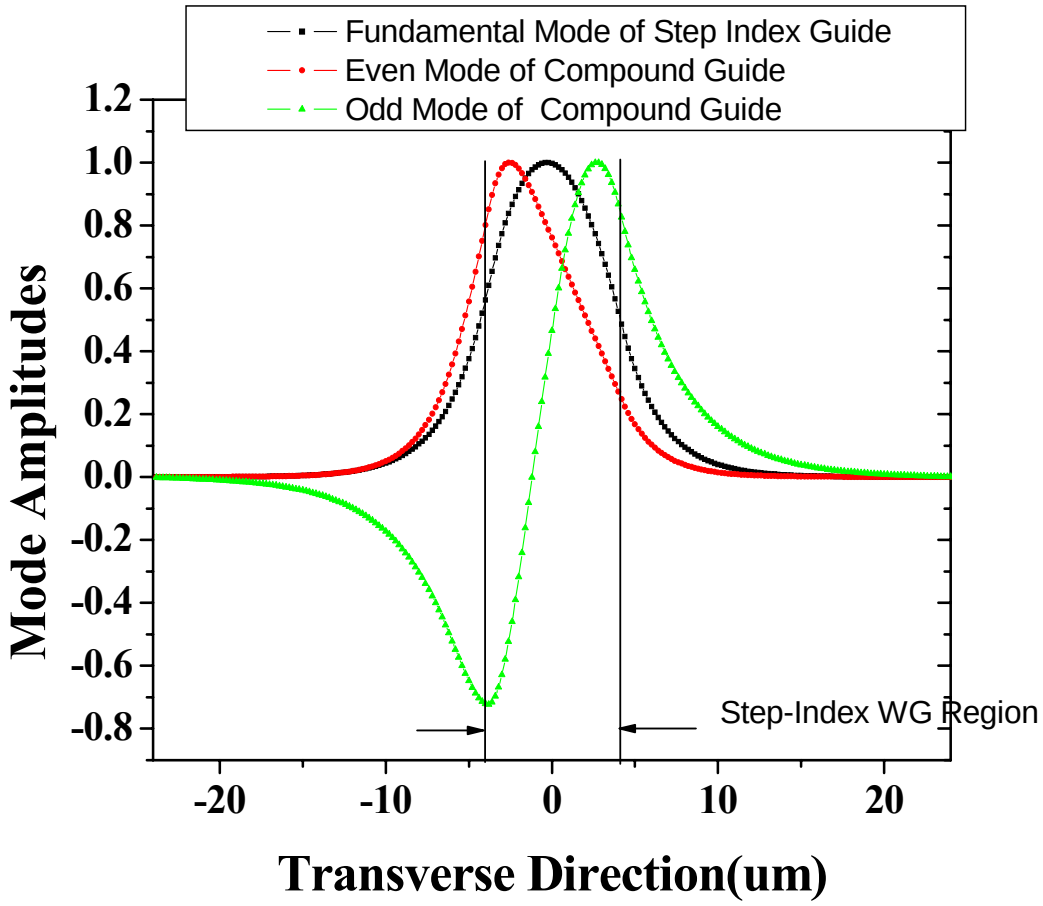

Figure 21-Even and Odd Guided Modes In the Tap Structure at Peak Refractive Index Change-0.005

There are two mechanisms to explain the radiation loss. Firstly, when the peak refractive index change is very small, the light profile will shift from the center of the through guide to the tap guide causing mode mismatch. Secondly, when the peak refractive index change is large, because the coupling between the excited even and odd mode, light power switch back and forth between through guide and tap guide. So, at the end of the tap region, due to lack of guiding, the power in the tap guide will leak out as radiation loss.

3.3.2 Strong index change situation

In this section, we first examine the index change induced by ion implantation is strong enough to support a guided mode at 1550 nm. In this case, we study optical loss due to the length L of the tap structure when other variables Rp , ΔRp , Δn_{peak} are fixed in this simulation, we set the projection range Rp =28um, i.e. at the core and lower cladding interface; ΔRp =1.35um and Δn_{peak} =0.005. Fig.22 and 23 shows the 2-D and 3-D transverse index profile at this configuration.

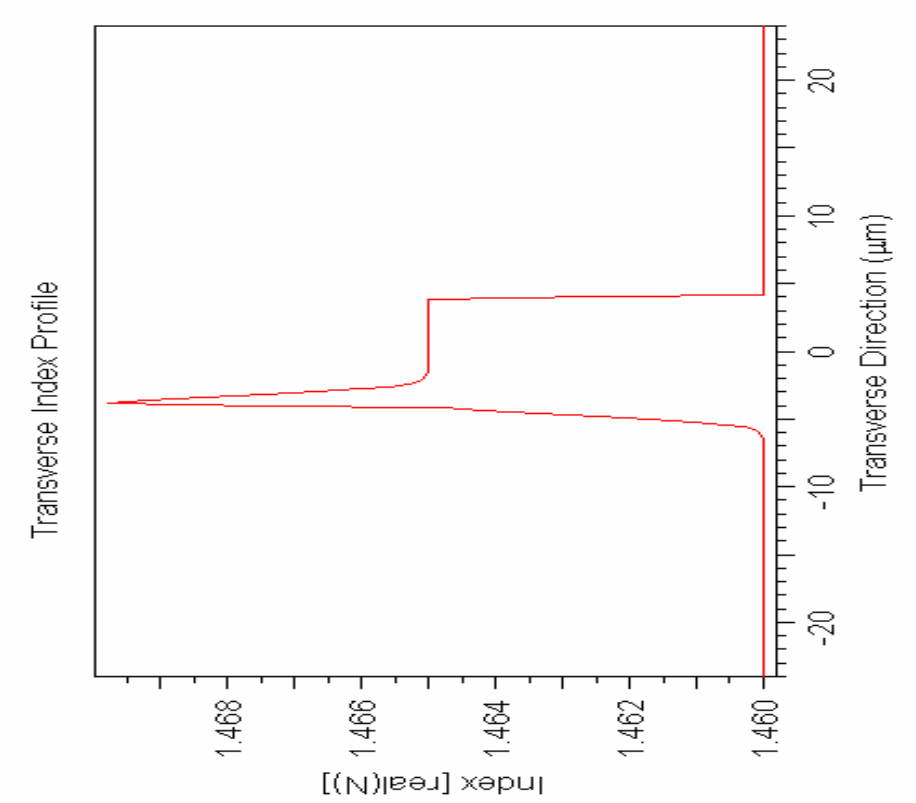

Figure 22-2D Transverse Index Profile

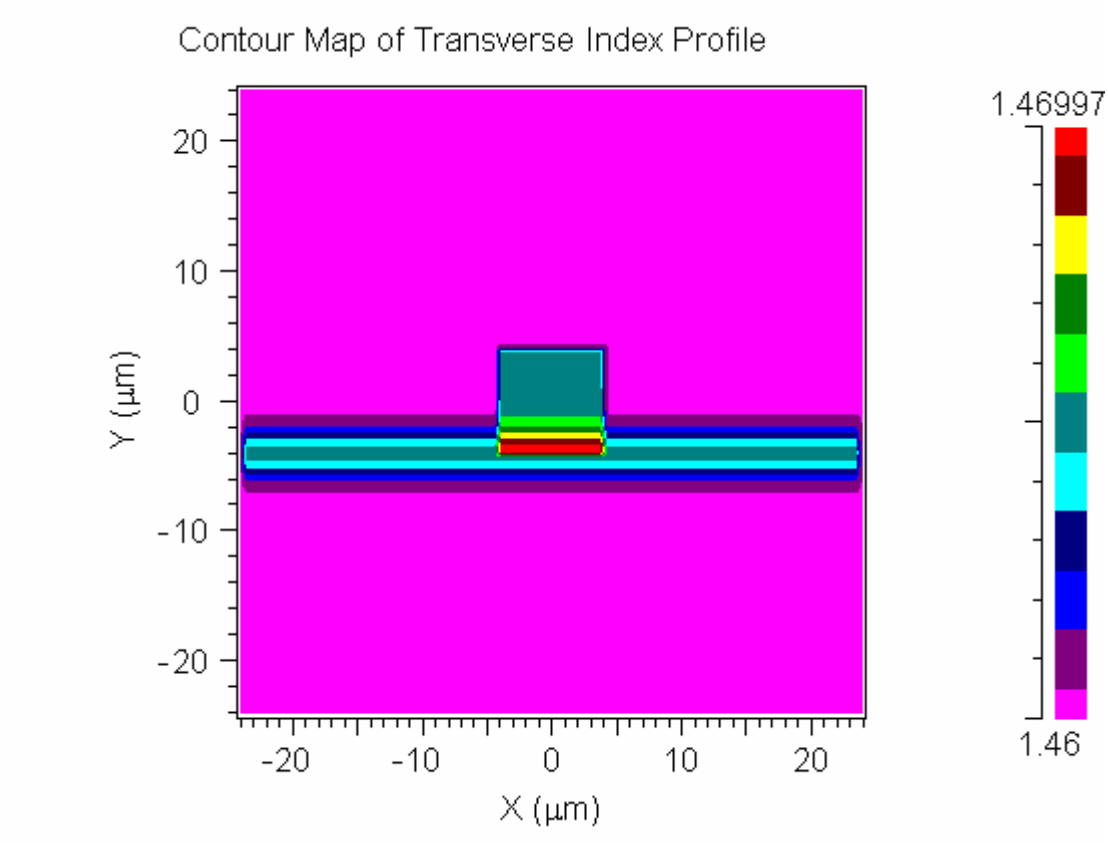

Figure 23-3D Transverse Index Profile

Figure.24 shows the optical field coupling effect between the original step index waveguide (upper blue guide) and the ion induced Gaussian index waveguide(lower green guide).

BeamProp simulations indicates along the tap length, some of the energy in the upper guide is seen to shift from the upper guide region to the lower guide region, and after a certain period this energy is then shifts back to the upper guide region before exiting the tap. The specific period T here is 500um.

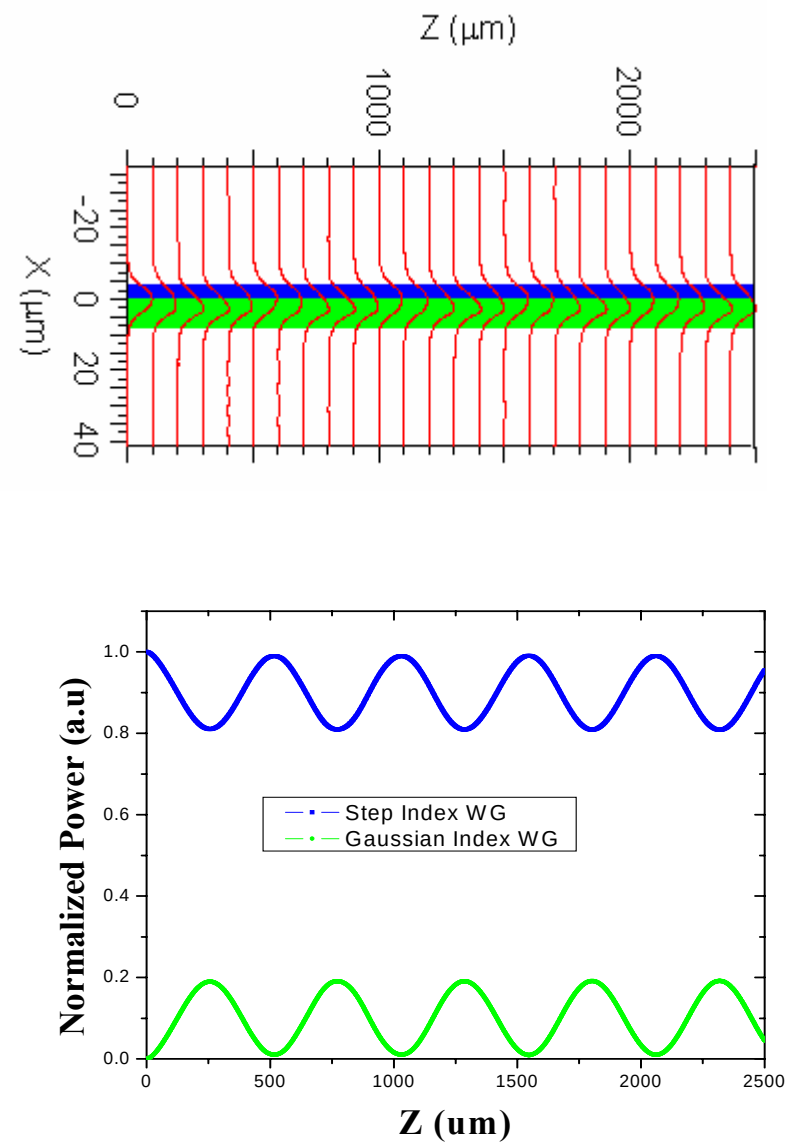

Figure 24-Upper Guide and Lower Guide Coupling Effect

When the tap length equals to half of the period (L=250um), maximum loss (20.3%) is observed where the maximum coupling between the upper and lower guide occurs. Figure.25 shows the coupling effect and field distribution at this condition where tap starts from 100um and ends at 350um.

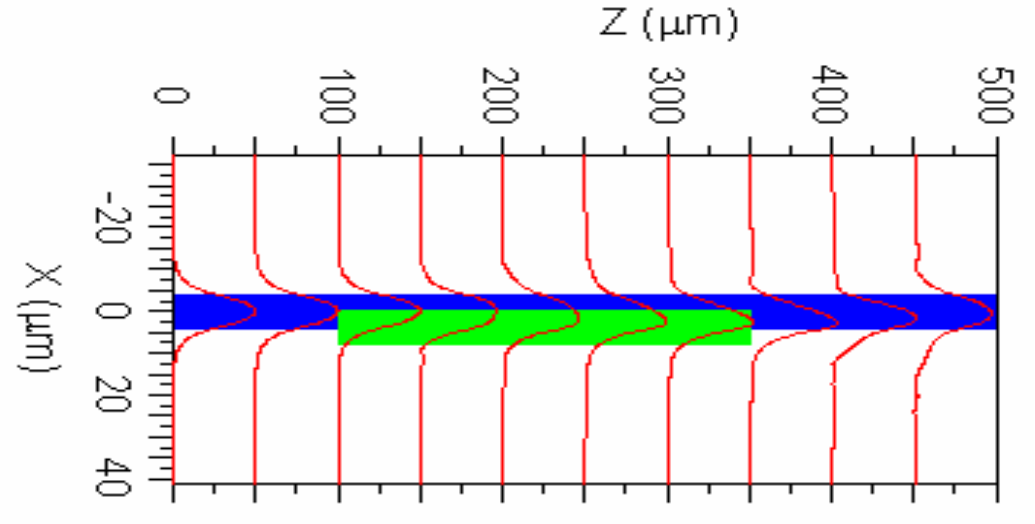
Z (μm)
0
100
200
300
400
500
X (μm)
-20
0
20
40

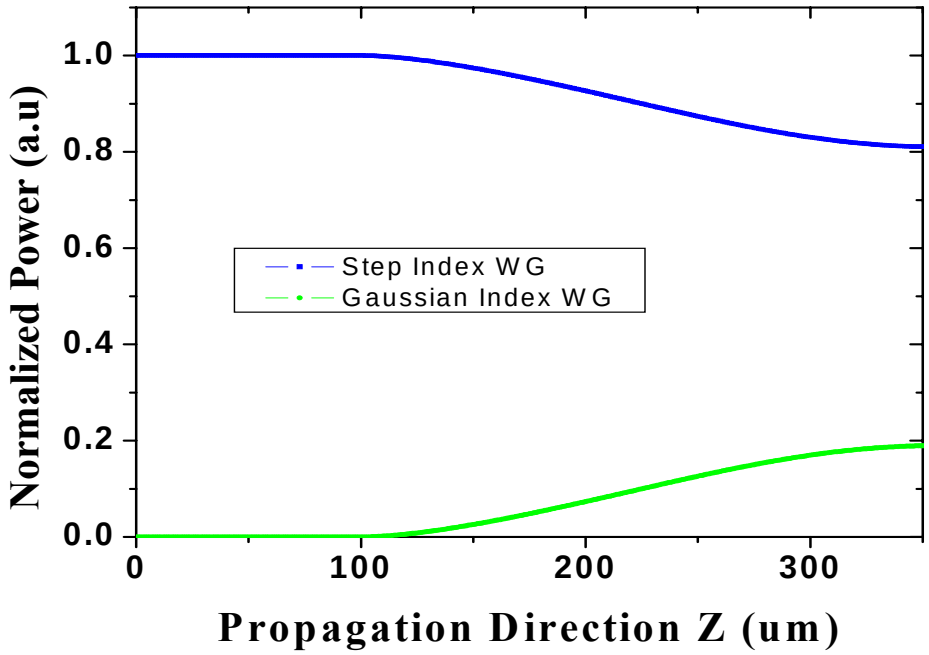
Normalized Power (a.u)
1.0
0.8
0.6
0.4
0.2
0.0
Step Index WG
Gaussian Index WG
0
100
200
300
Propagation Direction Z (um)

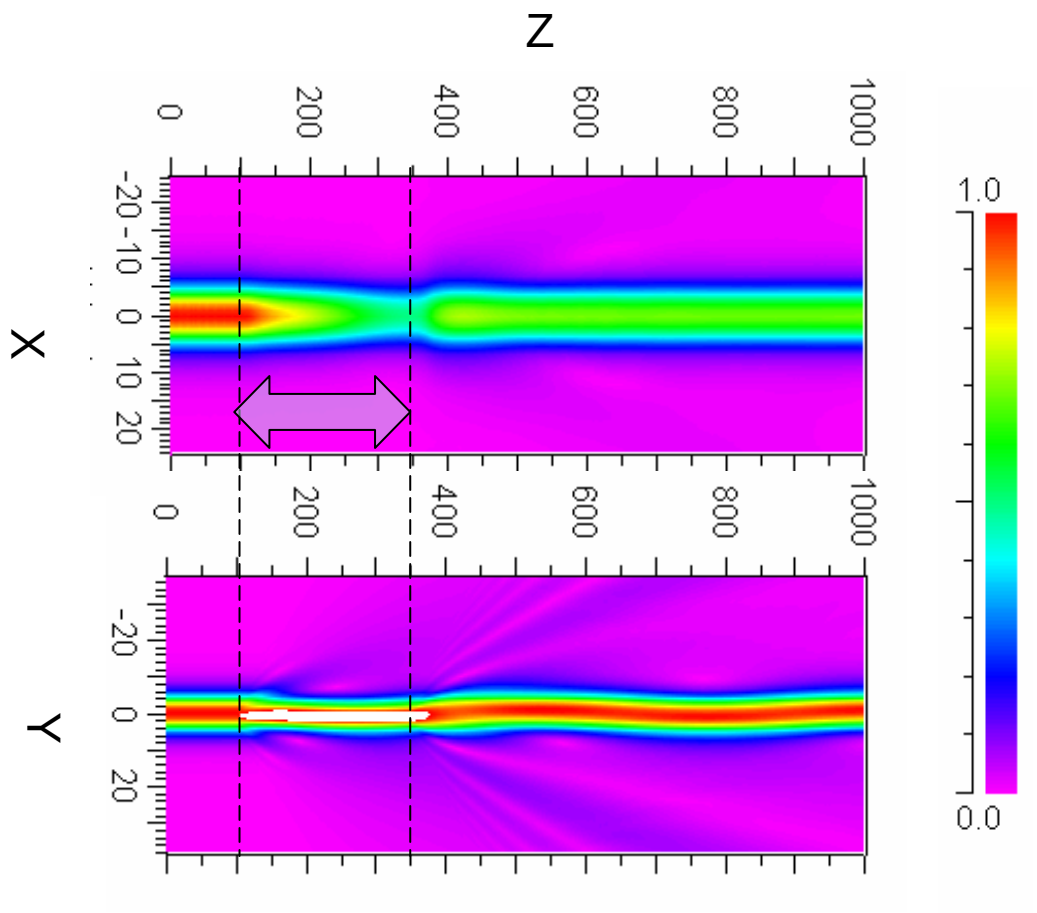

Figure 25-Maximum Coupling Between the Upper and Lower Guide (L=250um)

When the tap length equals to the full period (L=500um), minimum loss is observed where the minimum coupling between the upper and lower guide occurs. Figure.26 shows this coupling effect as well as the field distribution where tap starts from 100um and ends at 600um.

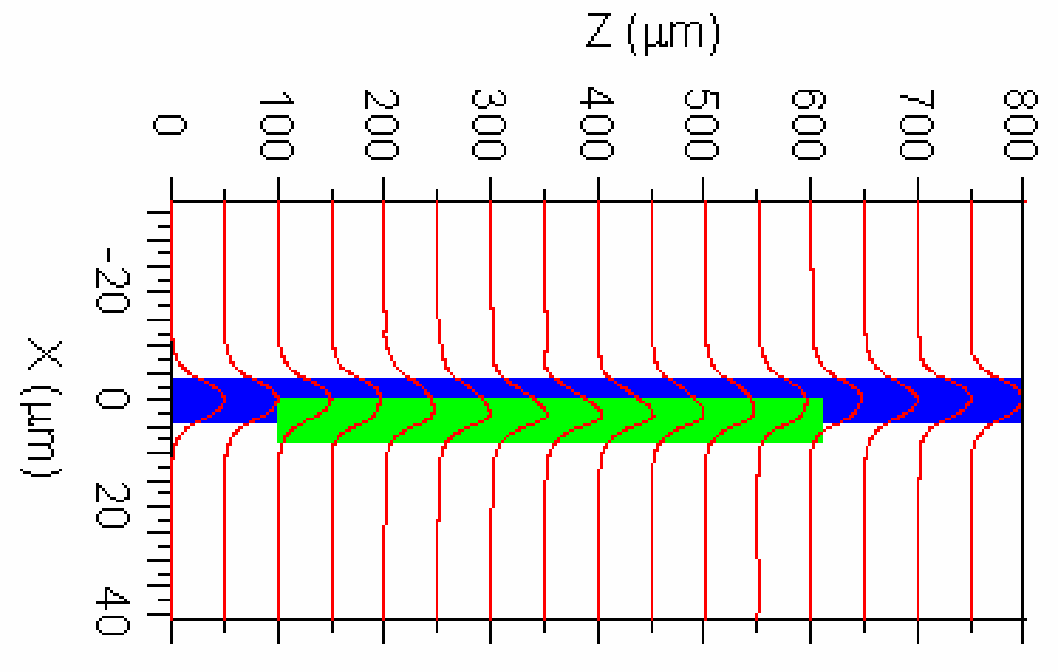
Z (μm)
0
100
200
300
400
500
600
700
800
X (μm)
-20
0
20
40

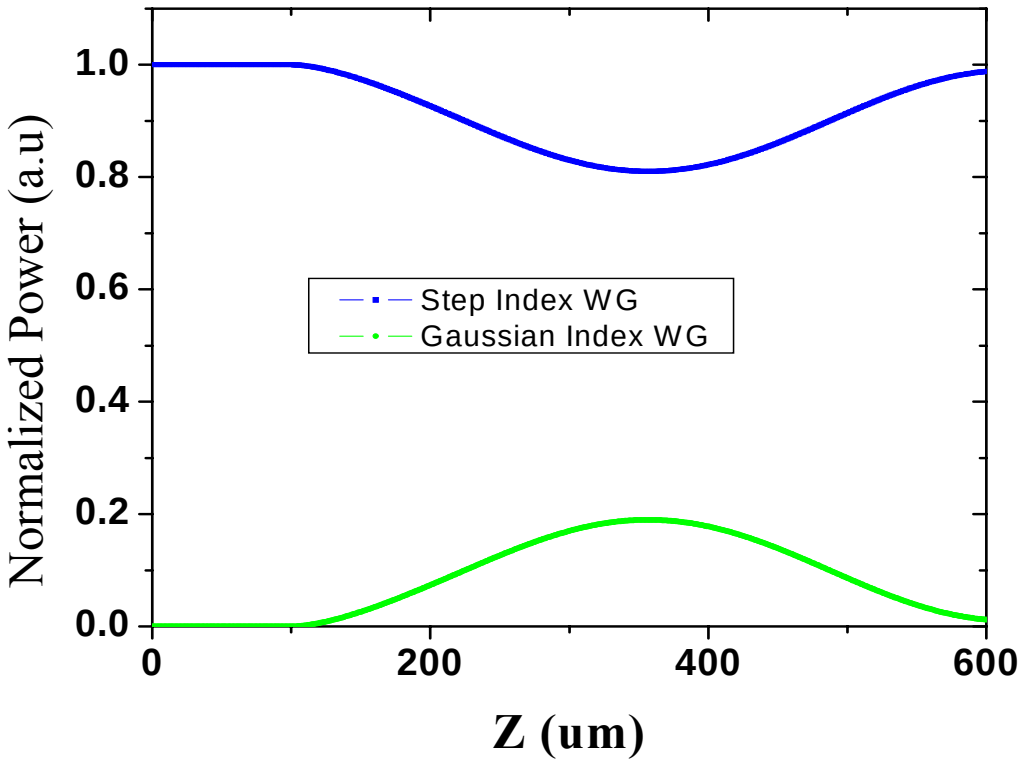
Normalized Power (a.u)
1.0
0.8
0.6
0.4
0.2
0.0
0
200
400
600
Z (um)
Step Index WG
Gaussian Index WG

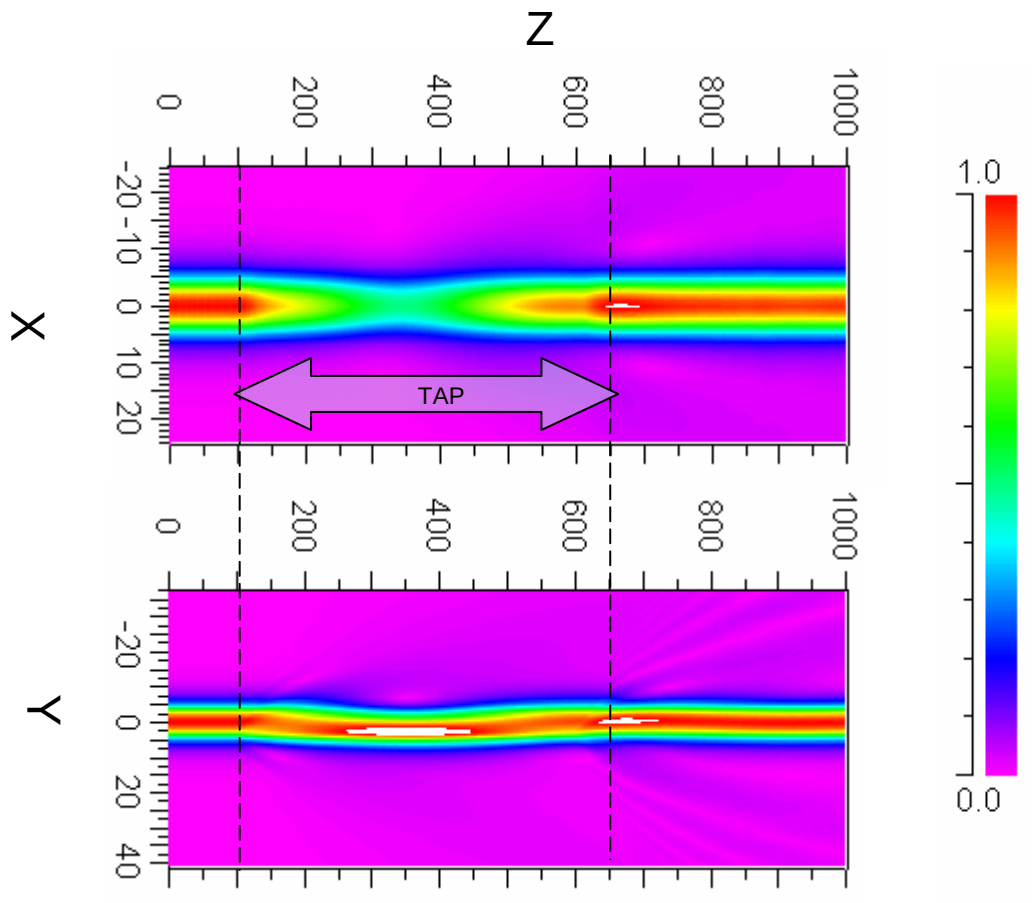

Figure 26-Minimum Coupling Between the Implanted Waveguide and Step Index Guide (L=500um)

From the above, at each tap, an adjustable fraction of the guided light is coupled into a silicon CMOS compatible photo detector by adjusting the length of the tap. Figure 27. shows 8% coupling occurs when tap length equals to 100um where taps start from 100um and ends at 200um.

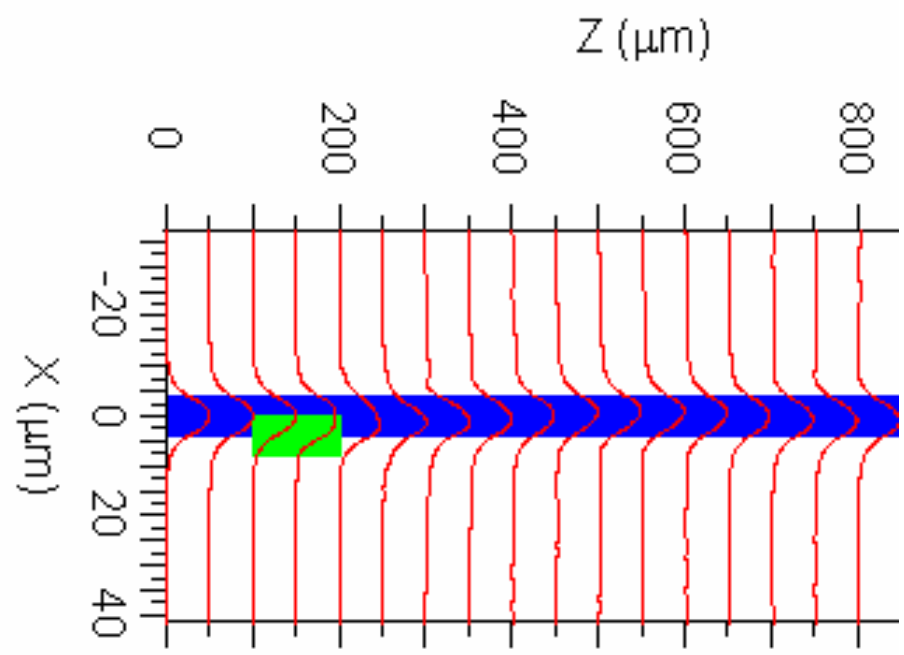
Z (μm)
0
200
400
600
800
X (μm)
-20
0
20
40

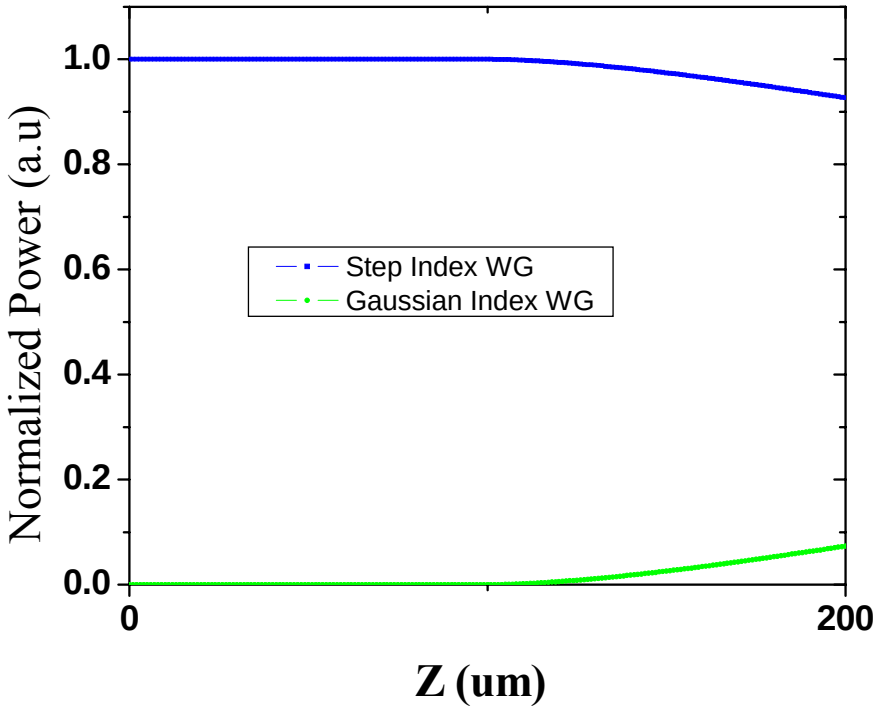
Normalized Power (a.u)
1.0
0.8
0.6
0.4
0.2
0.0
0
200
Z (um)
Step Index WG
Gaussian Index WG

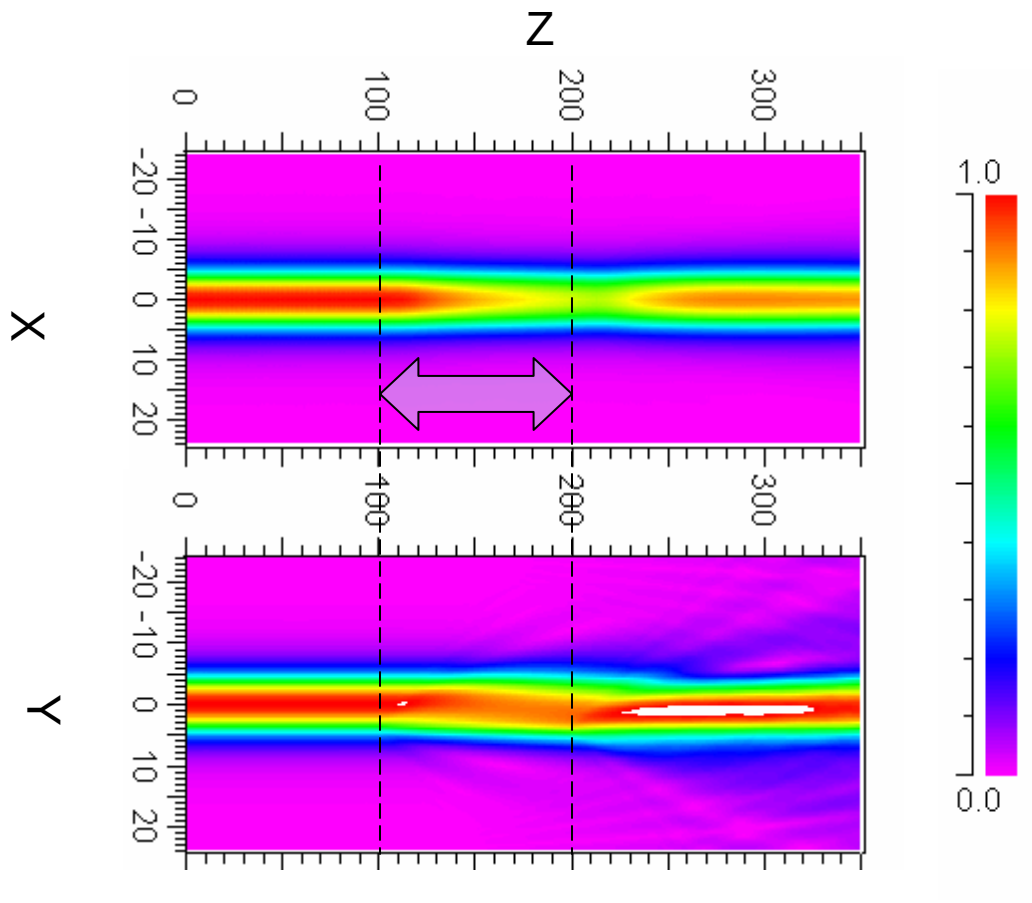

Figure 27-Adjustable Coupling by Adjusting Tap Length (L=200um)

3.3.3 Projection Range Rp Dependency Simulation

Here we fixed Δn_{peak} =0.005 and simulated the maximum coupling ratio and coupling length between the step index guide and induced Gaussian guide using different projection range Rp . As we can see from Figure.28, the closer the two waveguides, the larger the coupling ratio between them while the coupling length remains almost the same.

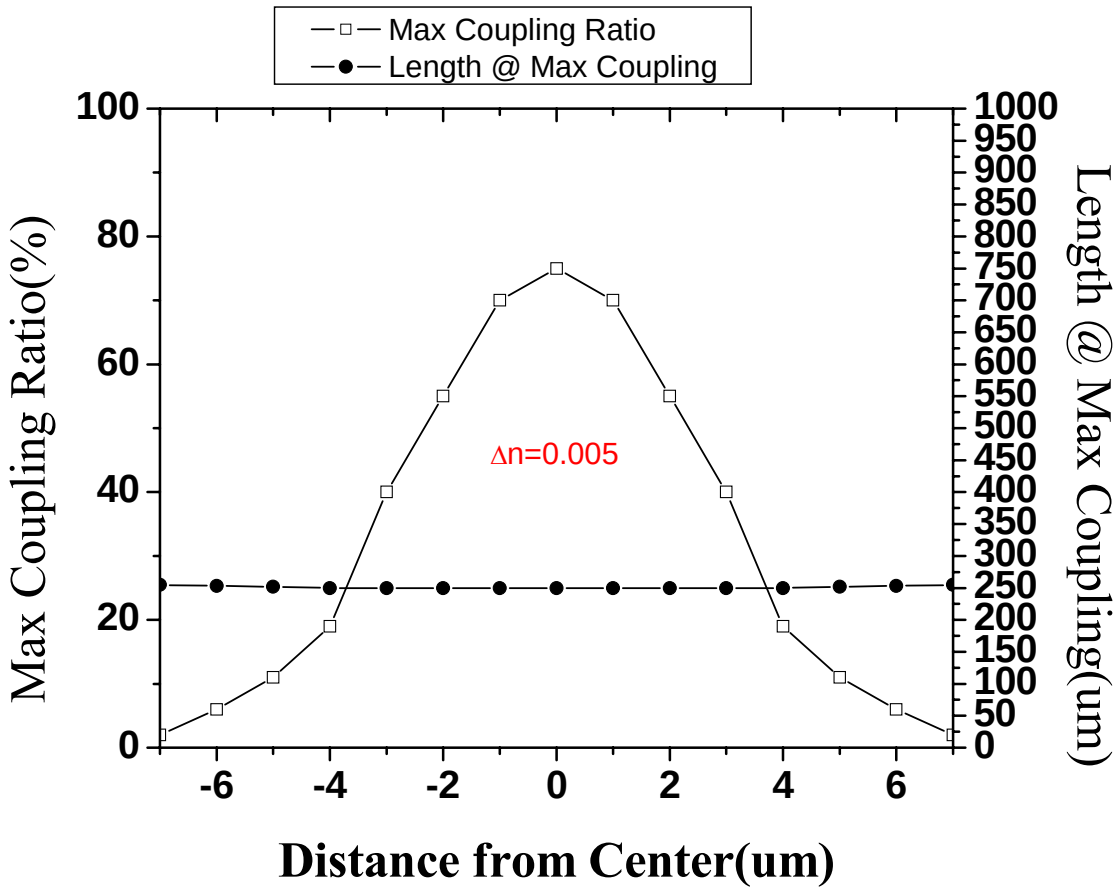

Figure 28-Coupling Ratio Dependency of Projection Range

Figure.29 shows the far field intensity distribution of both guides as a function of angle when projection range *Rp* locates at the center of the core. As you can see the acceptance angle of the Gaussian index waveguide is much smaller than that of the step index waveguide. Although more light is coupled from the step index guide to the Gaussian guide, the light is still confined within the step index guide instead of leaking out. The closer the two waveguides, the light coupled to the Gaussian guide is more confined in the step index guide (23).

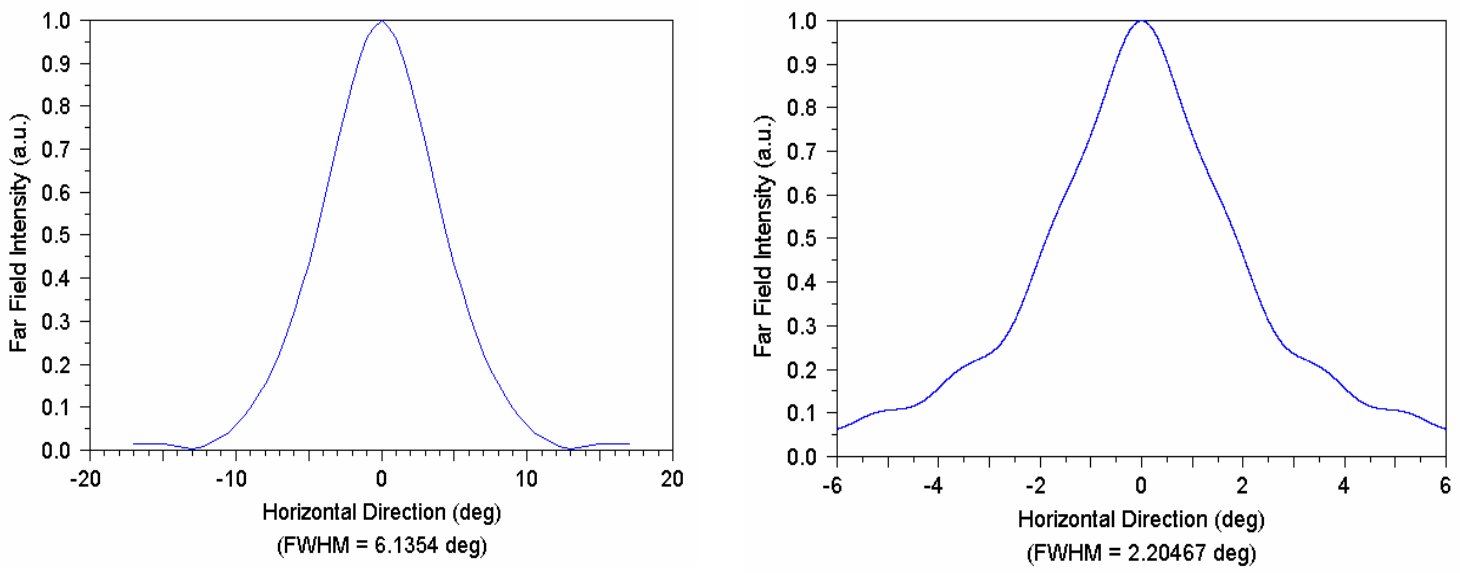

Figure 29-Field Intensity Angle Distribution of Both Guides

Based on both effects from the above, the closer the two waveguides, more light is coupled from the step index guide to the Gaussian guide, however, the light coupled to the Gaussian guide is more confined in the step index guide at the same time. So considering the overall total effect, simulation (Figure.30) shows the overall loss distribution as a function of projection range Rp.

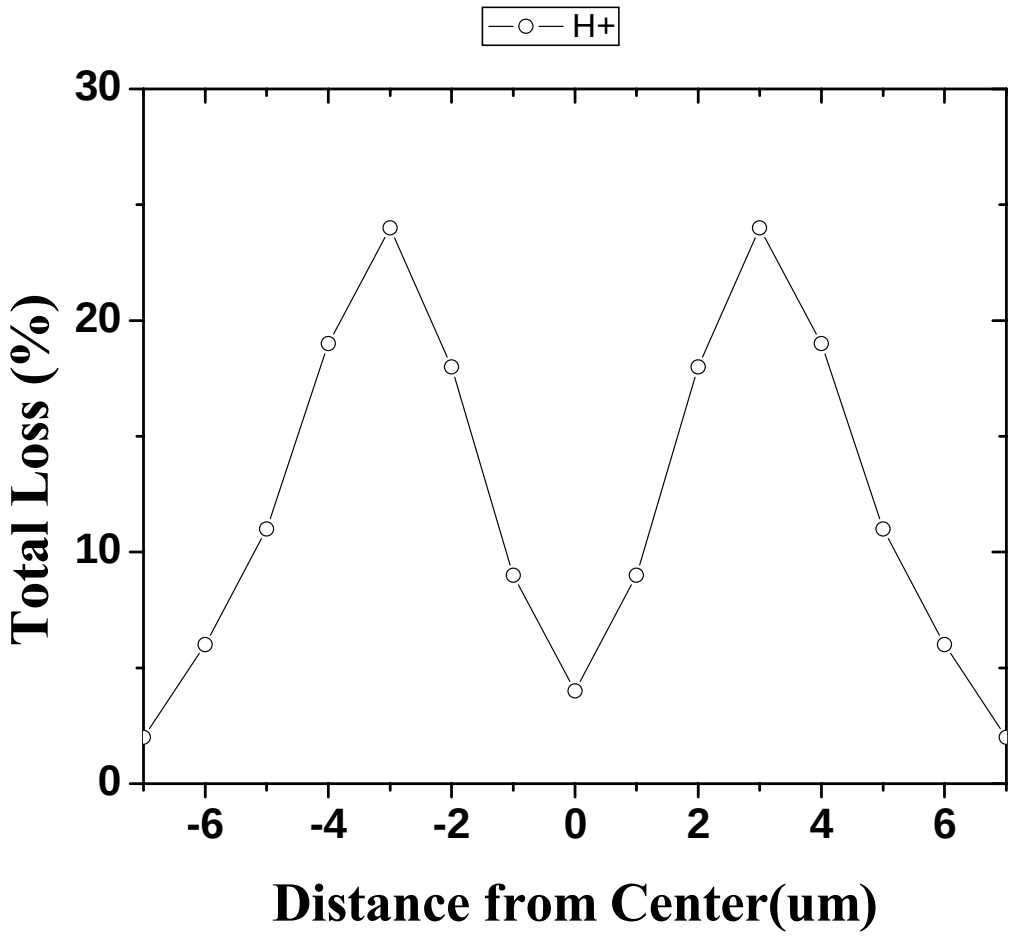

Figure 30-Total Loss Distribution With Different Projection Range

We can also use mode mismatch to explain the total loss distribution with different projection range Rp.

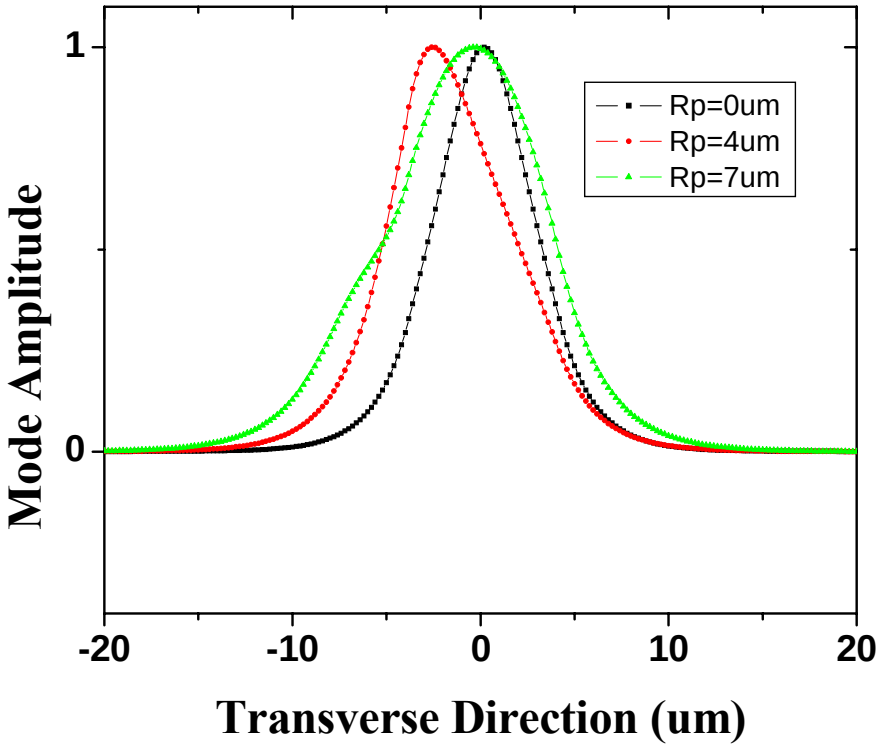

Figure 31-Mode Profile With Different Projection Range

Here we plot together (Fig.31) the computed transverse mode profile at different penetration depth. As we can see, when tap-guide locates at the through-guide core center (Rp=0), there is almost no mode mismatch resulting minimum radiation loss; when tap -guide locates at the through-guide core and cladding boundary(Rp=4), mode profile shift towards the tap waveguide resulting big mode mismatch and maximum radiation loss; when through- guide and tap-guide separate further apart (Rp=7um), mode profile shift back to the through-waveguide and reduce the mode mismatch resulting less radiation loss.

3.3.4 Δ n peak Dependency Simulation

Here we fixed tap length L=250um; the projection range Rp =28um; ΔRp =1.35um and simulated the total loss dependency of variation of peak refractive index change.

Here we show the fundamental mode distribution with different peak refractive index change from 0.001 to 0.005 in Fig.32. as we can see, the higher the refractive index change, the more shift light profile from the center of through waveguide to the implanted tap waveguide causing more mode mismatch and radiation loss.

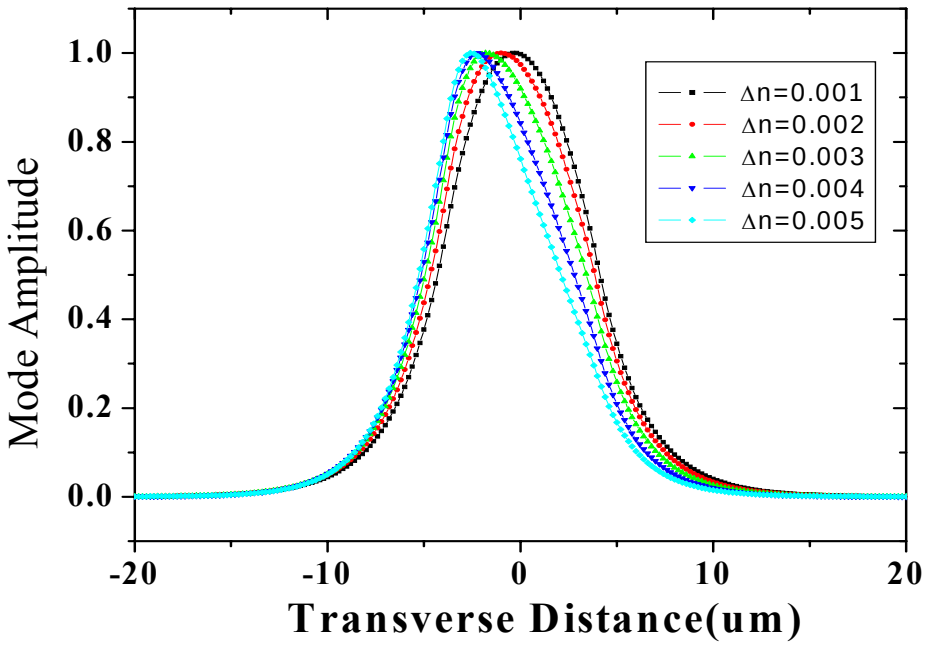

Figure 32-Mode Distribution of Different Implanted Peak Refractive Index Change

Figure.33 also shows that the radiation loss is proportional to the Δ n peak from the simulation results.

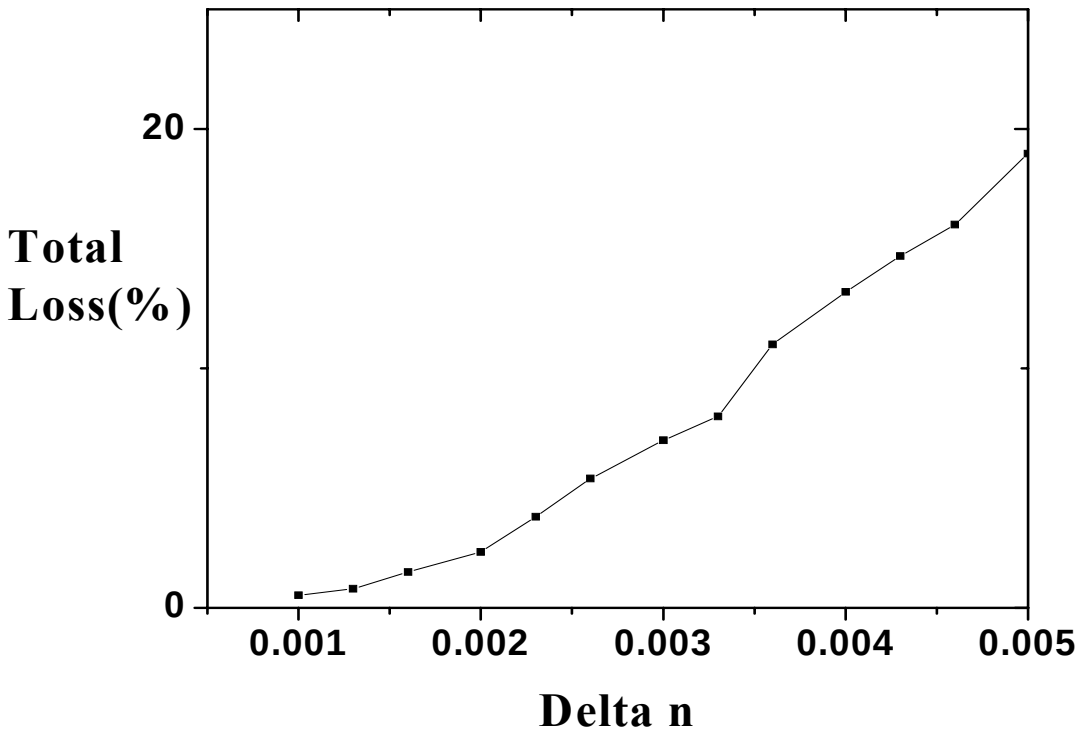

Figure 33-Total Loss vs. Peak Index Change

Based on the above discussion, we can adjust the fraction of the tap signal by controlling the 4 variables in the tap design, i.e. controlling the ion energy; ion species; ion dosage and tap length.

3.4 SERIES CASCADE OPTICAL TAPS

It should be pointed out that, in some application, it is desirable to design series of cascade optical taps. Some portion of the light is collected at each tap device and the remainder is passed on to other taps in a series fashion. Upon exiting the first tap structure, the light profile must match the single-mode input guide (i.e. when the blue line and green line align together) for transport to the next tap in the series. So, the position of the next tap must be after the point where blue line and green line cross as shown below in Fig.34.

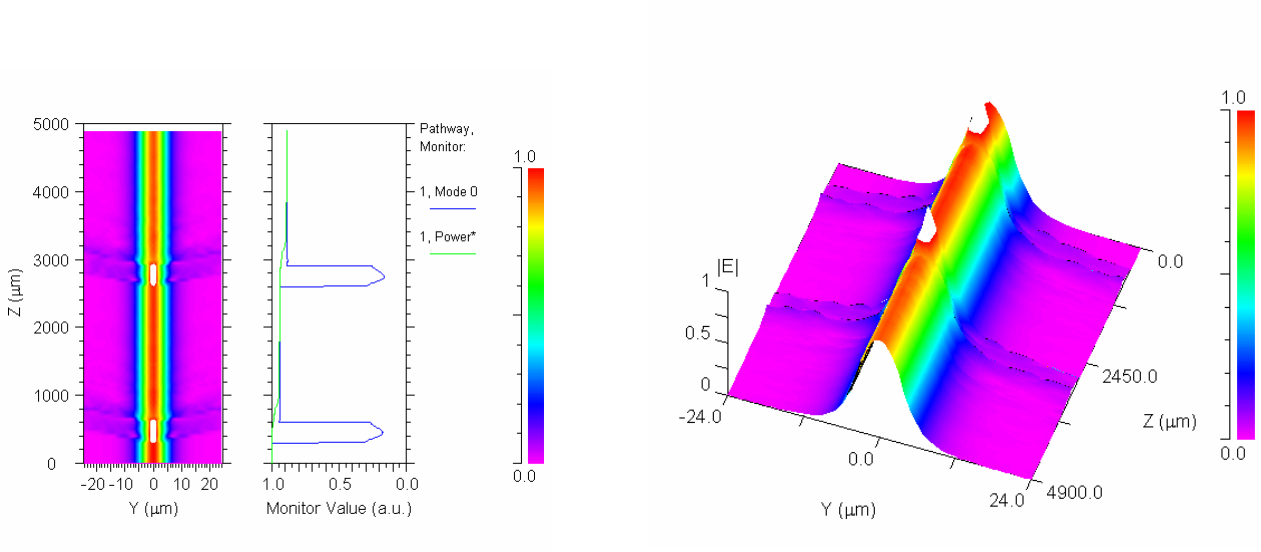

Figure 34-Realization of Series Cascade Optical Taps

3.5 DEVICE REALIZATION

Several device designs were considered for an ion-implantation based optical tap, and a very simple design was chosen for the initial demonstration. This device, illustrated in Fig 34. has protons implanted in the output AWG channels above which optoelectronics circuits were fabricated to collect the tap signal. Depending on different input wavelength, a portion of through signal of this wavelength will be extracted out vertically to the optoelectronics circuit at the tap in the corresponding output channel so as to realize the optical interconnect between the optical circuit and the electronics circuits. More complex designs will likely be required to achieve the performance required for practical interconnects, but this structure is an appropriate design in demonstrating and characterizing primary operation behavior.

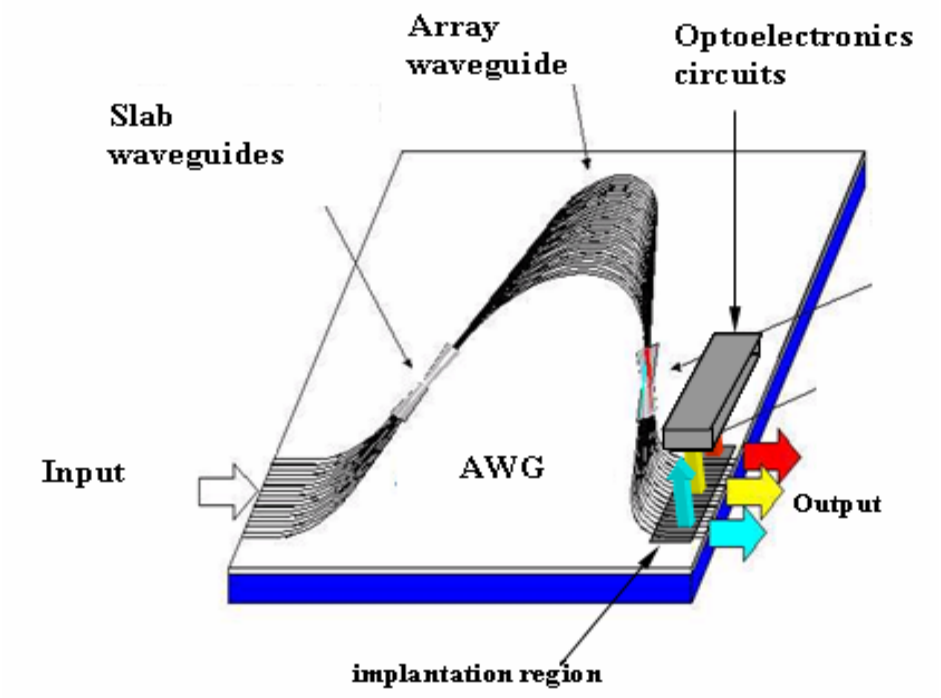

Figure 35-Ion Implantation tap in AWG device application

4.0 OPTICAL TAP FABRICATION AND DEMOSTRATION

To demonstrate the optical tap effect, we used the protons to bombard the commercially available FDM chips and got some preliminary results. As shown in Fig.36, the upper and lower cladding material is made of fused silica SiO2 with refractive index of 1.46. The average upper cladding thickness of our testing samples is around 21.5 um. The core is made of 3% Ge doped SiO2 with slightly higher index 1.465 with Δn=0.005. The width of core is 8um. Based on previous simulation and calculation, we use implantation dosage of $5\times10^{16} ion/cm^3$ and choose 1.25 MeV, 1.35 MeV, 1.45MeV, and 1.55MeV as our implant energies to bombard 4 different FDM chips. This results in a projection range about 21um and peak refractive index change Δn_{peak} =0.005 .This condition will make the penetration depth of the protons just touch the boundary between the upper cladding and core.

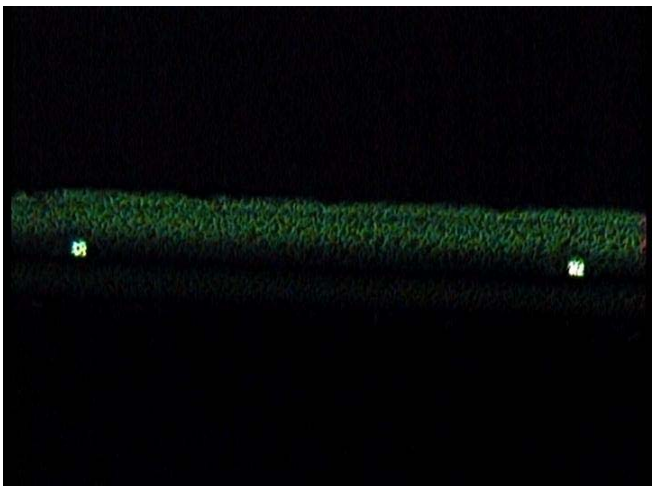

Figure 36-Cross Section of Commercially available FDM chip used in the experiments

After the ion implantation, a 3-D profile measurement is taken to verify the location and to measure the length and depth of the ion implantation.

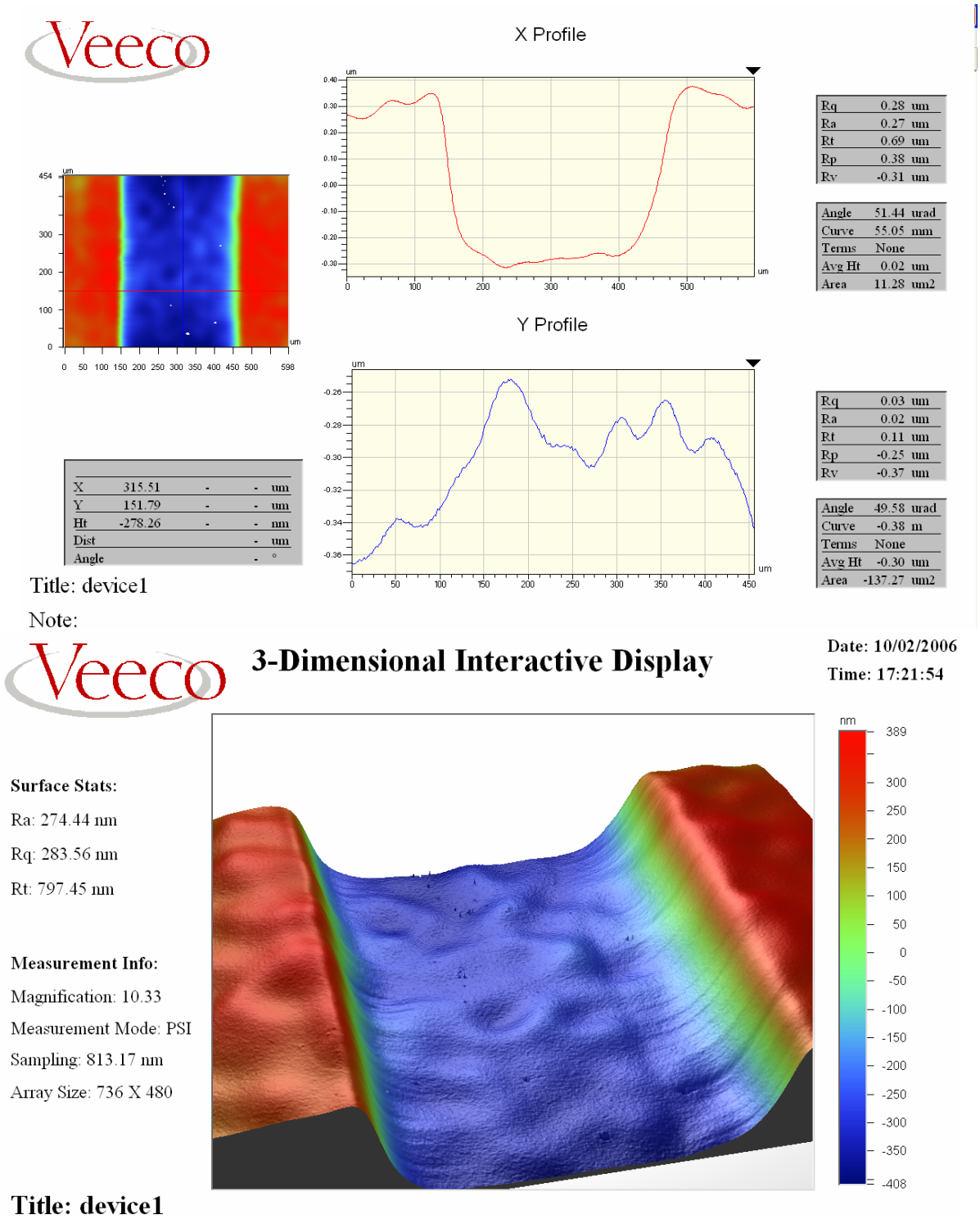

Figure 37-3D Profile of the FDM chip after the Ion Implantation Process

As seen from Fig.37, the average length of the ion implantation region is around 315.51 um with a depth about 0.6 um. After the implantation, a single mode fiber is bonded to the FDM chip via the V-Grove assembly and a diode red laser (2.5mW, 632nm) is then directly launched into the waveguide for a visual inspection on optical tap effect from the top view as shown in Fig.38.

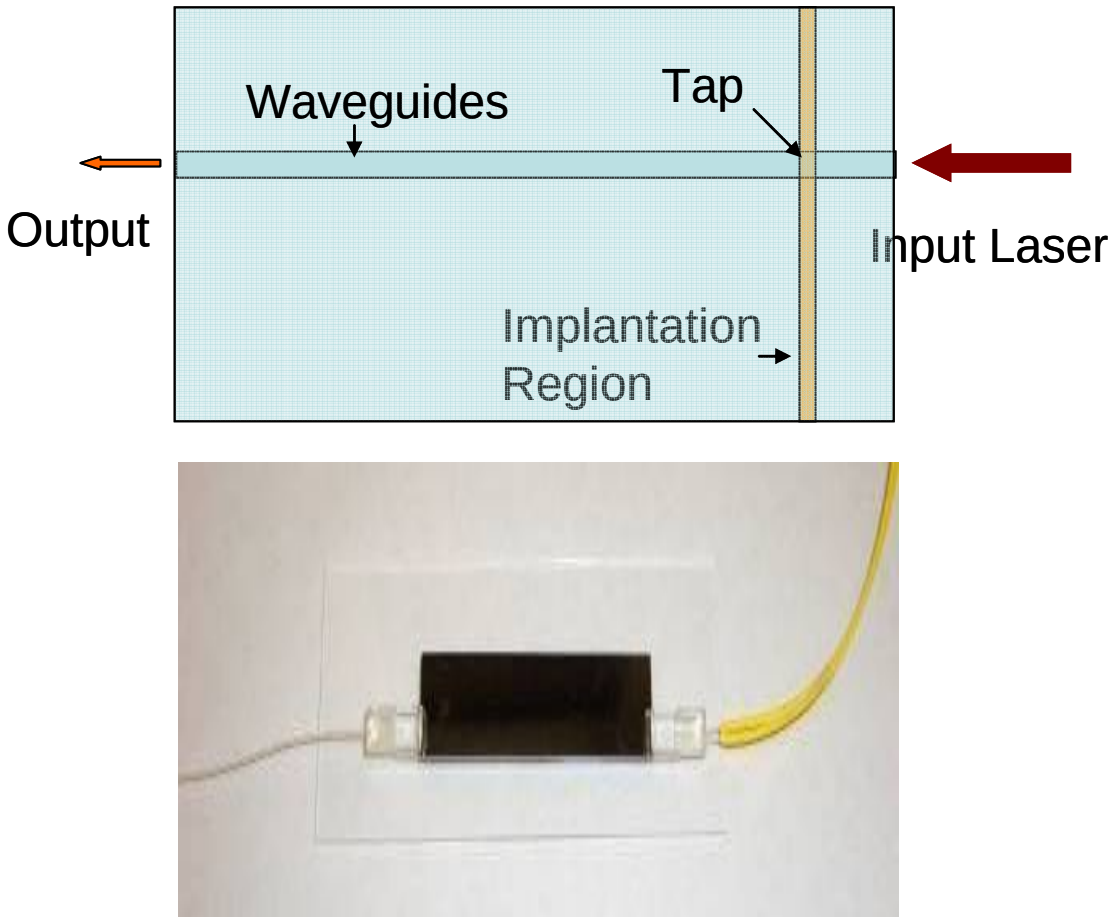

Figure 38-Visual Inspection of Optical Tap Effect

Fig.39 and 40 show the comparison top view pictures of the FDM chip before and after the ion implantation. Light tapping is clearly observed at the optical tap position.

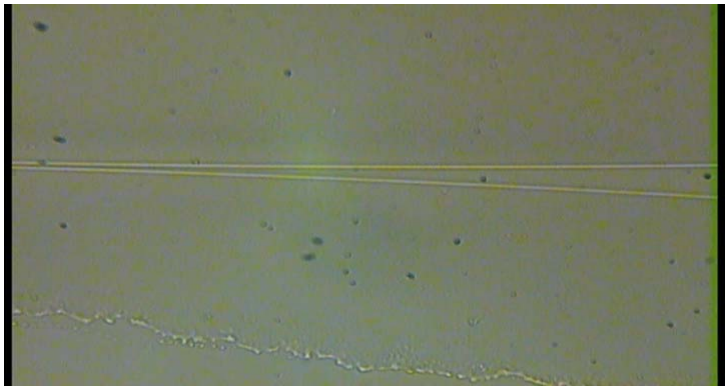

Figure 39-Top View Picture of the FDM chip before Ion Implantation

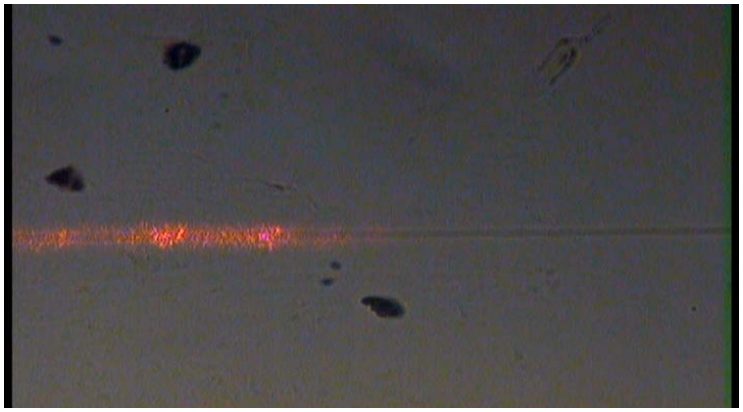

Figure 40-Top View Picture of the FDM chip after Ion Implantation

To find out the relationship between the through signal and the tap signal, we need to vary the input laser power. To do this, we misalign the input laser with the waveguide along the FDM chip width direction(as seen the X direction in Fig.13) and measure the tap signal intensity

and output signal intensity at the same time. The average of normalized intensity of both tapping signal and output through signal is plotted together in Fig.41. As we can see when the tap signals increase, the through signal also increases; when the tap signals decrease, the through signal also decreases. It is very clear that the change of the tap signal can effectively represent the change of the through signal and they have the same trend. This proves that the ion-implantation tap is functioning.

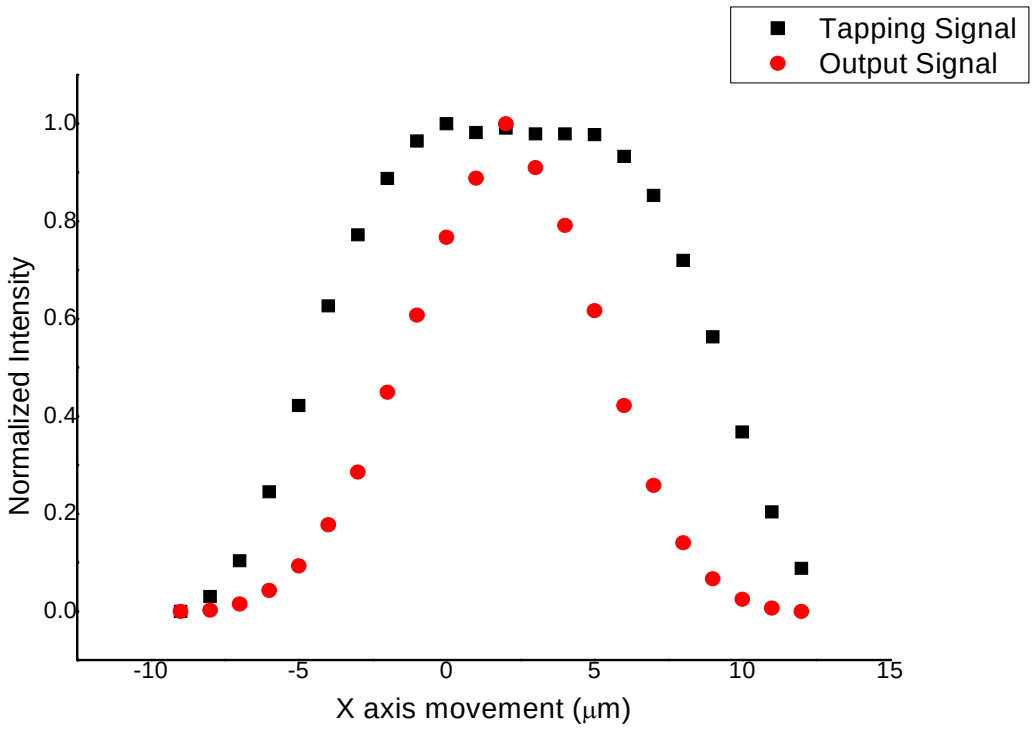

Figure 41-Comparison between the Output Through Signal and Tapping Signal

5.0 ANALYSIS

5.1 SUMMARY

In summary, we have determined a promising candidate technology for economical maximal-performance integrated optic waveguide taps on CMOS circuits. The design extracts the maximum optoelectronic receiver performance from the silicon system by coupling a low-loss vertical ion-implantation induced optical tap design with traveling wave detector technology. An especially attractive feature of the technology is that it can utilize well-established ion implantation technique to form a new optical waveguide in an already established wafer based planer photonic device. The advantage of ion implantation approach for optical tap fabrication is as follows:

1. Not Invasive, “Post” Processing;
2. Easy to Control, Adjustable Variables;
3. Vertical Tapping solved the real estate constraint;
4. Easy to integrate with CMOS devices.

To adjust individual tap coupling ratios, a combination of tap length adjustment and the use of different ion implantation energy and dosage has been presented. Applications targeted by the technology include high bandwidth optical distribution of signals at the electronic circuit

board and multi chip levels as well as the highly cost sensitive fiber to the home and fiber to the desk applications.

5.2 FUTURE WORK

As shown below, to collect the tapped signal, we can either put a PD (Photo Detector) array on top of the tap or directly integrate a CMOS PD below the tap in the Si substrate. But the length of the PD has to be longer than the distance from the start of the tap to the intersection of the blue and green line where the light recovers totally back into the core to collect all the light been tapped out.

In the second case, because the big refractive index difference between the Si substrate and SiO2 cladding, from Frenel's Equation the reflectance at the silica and silicon interface is given by:

$$R = \left(\frac{n_{silica} - n_{silicon}}{n_{silica} + n_{silicon}} \right)^2 = \left(\frac{1.46 - 3.5}{1.46 + 3.5} \right)^2 = 16.9\%$$

This means a large portion of the light will be reflected back up, and an AR spacer might be needed. Fig.41 shows the proposed design of the AR spacer.

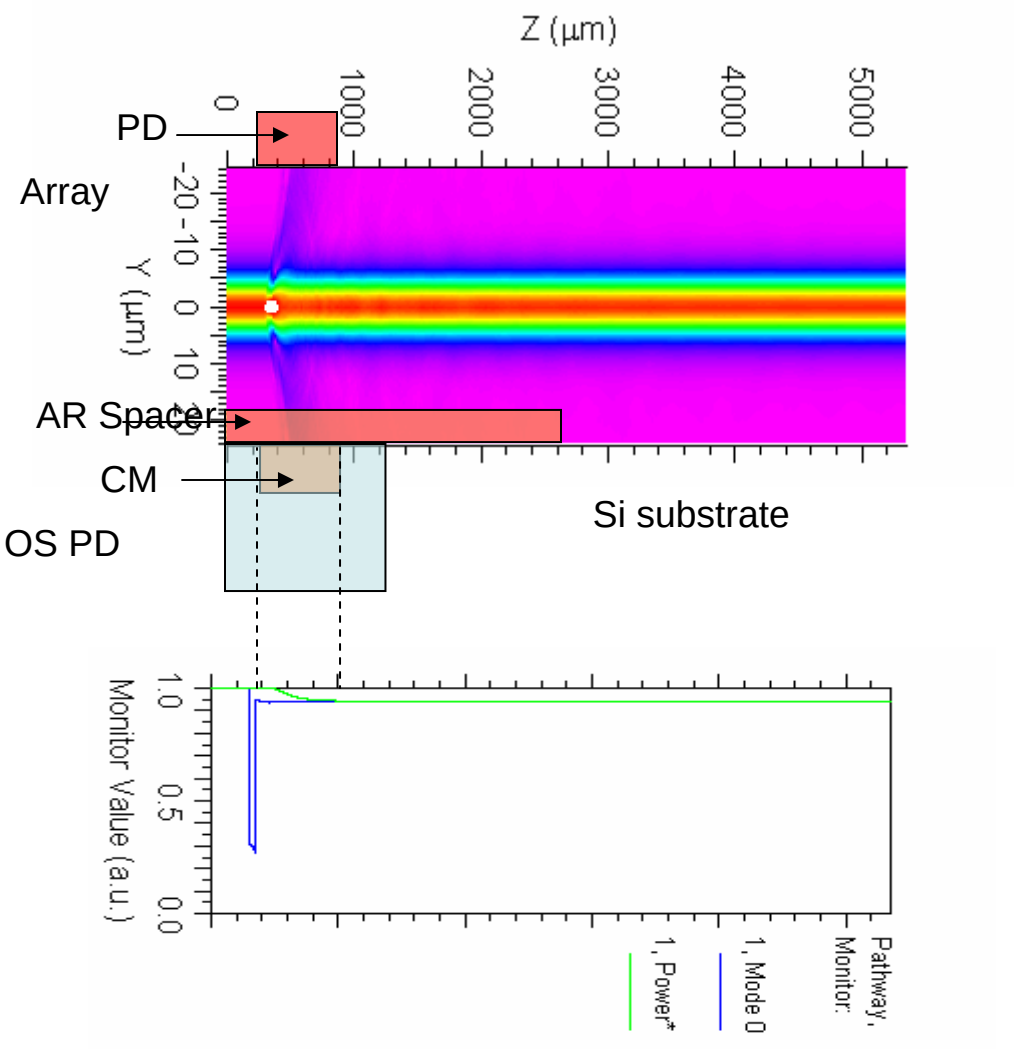

Figure 42-Proposed Design of Optical Tap Device with AR Spacer

APPENDIX

COPYRIGHT PERMISSION LETTER FROM IEEE

Dear Zhuo:

This is in response to your letter below, in which you have requested permission to reprint, in your upcoming thesis/dissertation, IEEE copyrighted figures. We are happy to grant this permission.

Our only requirements are that you credit the original source (author, paper, and publication), and that the IEEE copyright line (© [Year] IEEE) appears prominently with each reprinted figure.

Best regards
Tony VenGraitis, IPR Specialist

-=-

IEEE Intellectual Property Rights Office
445 Hoes Lane, Piscataway, NJ 08855
Telephone: +1 732-562-3966
Fax: +1 732-981-8062
w.hagen@ieee.org

BIBLIOGRAPHY

1. S. Natarajan, C. Zhao, R. T. Chen, "Bi-directional optical back plane bus for general purpose multi-processor board-to-board optoelectronic interconnects," J. Lightwave Technol, 1995. 13 (6):p.1031-1040.

2. J. Moisel, J. Guttmann, R. Bogenberger, "Optical backplanes with integrated polymer waveguides," Opt. Eng, 2000. 39 (3):p. 673-679.

3. V. Stinger, F. R..Beyette, Jr., "Design and analysis of an optical waveguide tap for silicon CMOS circuits," Journal of Lightwave Technology, 2002.20(2):p. 277-284.

4. T.E.Van Eck, A.J. Ticknor, R.S.Lytel, G.F. Lipscomb, "Complementary optical tap fabricated in an electro-optic polymer waveguide," Appl. Phys. Letter, 1991.58(15):p.1588-1590.

5. Corning Incorporated, Corning , New York, European Patent EP 1115012A1 , 2000,

6. R.Yoshimura, M. Hikita, M. Usui, S. Tomaru, S. Imamura, "Polymeric optical waveguide films with 45 degree mirrors formed with a 90 degree V-shaped diamond blade," Electronics Letters, 1997.33(15):p. 1311-1312.

7. S. Imamura, R. Yoshimura, T. IZAWA, "Polymer channel waveguides with low loss at 1.3um," Electron Letters, 1991.27(15): p.1342-1343.

8. Kaneko, A. Hikita, M. Imamura, S. And Kihara, M, "Flexible multimode polymer waveguides for optical interconnections," Fifth Int. Conf. Plastic Opt. Fibers Appl, 1996, p.113-119.

9. Tewksbury, S. et al., "Optical clock distribution in electronic systems," Journal of VLSI Signal Processing 16, 1997, p 225-246.

10., "Ridge waveguide optical taps on silicon substrates," Proceedings of SPIE vol.5181, 2003

11. V. Stinger, F. Beyette, "Silicon CMOS based vertical multimode interference optical taps," proceedings of SPIE Vol.4435 (2001)

12. J.P.Uyemura, "Introduction to VLSI Circuits and Systems", p.115-146, John Wiley&Sons, 2001

13. S.Ghandhi, "VLSI Fabrication Principles", John Wiley&Sons, 1994, p.368-451

14. J.Zeigler, R.Lever, "Channeling of Ions near the silicon <100> axis," Appl. Phys.lett. 46(358) (1985)

15. D.R. Zrudsky, "Channeling control in ion implantation," Solid State Technol, 1988, p69

16. A.Roberts and M.L. von Bibra, "Fabrication of buried channel waveguides in fused silica using focused MeV proton Beam Irradiation," Journal of Lightwave Technology, 14(11),1996,p.2554-2557.

17. M. Fujimaki, Y. Ohki, J. L. Brebner, S. Roorda, "Fabrication of long-period optical fiber gratings by use of ion implantation," Optics Letters, 25(2), 2000, p.88-89.

18. S. Pilevar, B. Lee, K. Grabowski, D. Knies, "Ion beam modification of optical components: a new fabrication and tuning technique for creating Mach-Zehnder interferometer based coarse WDM components," Internal Communication

19. www.srim.org

20. Marcuse, D. “Mode conversion caused by surface imperfections of a dielectric slab waveguide,” B.S.T.J, 1969.48(10), p.3187-3216

21. Marcuse, D. “Radiation losses of dielectric waveguides in terms of the power spectrum of the wall distortion function, B.S.T.J1969. 48(10), p.3233-3242.

22. Marcuse, D. and Derosior, R.M. “Mode conversion caused by diameter changes of a round dielectric waveguide,” B.S.T.J B.S.T.J1969. 48(10), p. 3217-3232.

23. B.Saleh, M. Teich. “Fundamentals of Photonics,” John Wiley&Sons, 1991